SEPARATION OF CARBON DIOXIDE FROM NITROGEN AND WATER IN FLUE GAS STREAMS

A Senior Scholars Thesis

by

HILDA A. MERA

Submitted to Honors and Undergraduate Research
Texas A&M University
in partial fulfillment of the requirements for the designation as

UNDERGRADUATE RESEARCH SCHOLAR

May 2012

Major: Chemical Engineering

SEPARATION OF CARBON DIOXIDE FROM NITROGEN AND WATER IN FLUE GAS STREAMS

A Senior Scholars Thesis

by

HILDA A. MERA

Submitted to Honors and Undergraduate Research
Texas A&M University
in partial fulfillment of the requirements for the designation as

UNDERGRADUATE RESEARCH SCHOLAR

Approved by:

Research Advisor: Perla B. Balbuena
Associate Director, Honors and Undergraduate Research: Duncan MacKenzie

May 2012

Major: Chemical Engineering

ABSTRACT

Separation of Carbon Dioxide from Nitrogen and Water in Flue Gas Streams.
(May 2012)

Hilda A. Mera
Department of Chemical Engineering
Texas A&M University

Research Advisor: Dr. Perla B. Balbuena
Artie McFerrin Department of Chemical Engineering

Grand Canonical Monte Carlo simulations (GCMC) are used to examine the adsorption isotherms of carbon dioxide, nitrogen, and water in metal-organic frameworks (MOFs). Molecular Dynamics (MD) simulations are used to determine the diffusion coefficients of carbon dioxide, nitrogen, and water in MOFs. The metal-organic frameworks studied are copper trimesate (Cu-BTC), zinc terephthalate (IRMOF1), and MIL-47, which belongs to the Materials of the Institute Lavoisier series. Diffusion coefficients are determined by the mean-square displacement method derived by Albert Einstein. The diffusion coefficients of each component in the flue gas are analyzed to examine the effect of temperature in diffusion coefficients and study the motion of the gases in the MOF. At thermal equilibrium, the radial distribution function of carbon dioxide, nitrogen, and water are obtained to find the position of atoms with respect to the metal sites of the MOFs. The selectivity for carbon dioxide in a gas mixture composed of carbon dioxide, nitrogen, and water is determined at room temperature. The selectivity for carbon dioxide in flue gas is found by considering the amount adsorbed of carbon

dioxide with respect to the amount adsorbed of nitrogen and the molar fractions of carbon dioxide and nitrogen in the flue gas. To account for the molecular interactions between the molecules in the flue gas and the metal-organic frameworks, van der Waals forces are accounted in this study. The Lennard Jones potential parameters for each atom in the metal-organic framework are obtained from the Dreiding force field. Location of carbon dioxide, nitrogen, and water relative to the metal atom in the MOF is observed using Material Studio 5.5 and Visual Molecular Dynamics. Based on the computational results, MIL-47 has the highest selectivity for carbon dioxide in gas mixture at room temperature because carbon dioxide strongly interacts with vanadium metal. Cu-BTC also shows high selectivity for carbon dioxide, whereas IRMOF-1 has lower selectivity for carbon dioxide.

DEDICATION

I would like to dedicate this undergraduate scholar thesis to my parents, Pedro Fernando Mera and Hilda Margarita Mera-Sosa, and my brother, Fernando Daniel Mera-Sosa.

ACKNOWLEDGMENTS

I would like to thank Dr. Perla Balbuena for her tremendous support in my research achievements. She has been a mentor since Spring of 2010, and she has inspired me to pursue my career goals. In the Summer of 2011 and the Fall Semester of 2011, Dr. Balbuena guided me in my research for the Undergraduate Research Scholar Program. In addition, I would like to thank Dr. Balbuena's research group. I would like to thank Jiamie Yu, Laura Mateos, Rafael Callejas-Tovar, Fredy Cabrales, and Juan Burgos for their support and encouragement. These students introduced me to Grand Monte Carlo simulations and Molecular Dynamics simulations.

NOMENCLATURE

a	Distance in the vertical axis of a unit cell in the Cartesian coordinate system
b	Distance in the horizontal axis of a unit cell in the Cartesian coordinate system
c	Distance in the inward axis of a unit cell in the Cartesian coordinate system
D_s	Diffusion coefficient
g(r)	Radial distribution function
x_{CO2}	Molar fraction of adsorbed phase of carbon dioxide
x_{N2}	Molar fraction of adsorbed phase of nitrogen
y_{N2}	Molar fraction of the bulk gas phase
y_{CO2}	Molar fraction of the bulk gas phase
$S_{ads(i/j)}$	Selectivity for i from i/j mixture
$S_{ads(CO2/N2)}$	Selectivity for CO2 from CO_2/N_2 mixture
ε	Depth of the potential well
ε_{ii}	Depth of the potential well for a homoatomic pair
ε_{ij}	Depth of the potential well for a heteroatomic air
k	Boltzmann's constant
σ	Average collision diameter
σ_{ii}	Average collision diameter for a homoatomic pair
σ_{ij}	Average collision diameter for a heteroatomic pair
q_C	Atom charge of carbon

q_N	Atom charge of carbon
e^-	Electron charge
N	Total number of molecules
V	Volume of system
V(r)	Lennard Jones potential
ρ	Density
T	Temperature
t	Time
P	Pressure
r	Radius of atom
y_i	Composition fraction of component i in gas mixture
y_j	Composition fraction of component j in gas mixture
x_i	Amount adsorbed mole fraction of component i
x_j	Amount adsorbed mole fraction of component j
α	Angle between b and c
β	Angle between a and c
γ	Angle between a and b
ν_B	Boltzmann's Constant

TABLE OF CONTENTS

CHAPTER Page

LIST OF FIGURES

FIGURE Page

FIGURE Page

FIGURE Page

LIST OF TABLES

TABLE Page

CHAPTER I

INTRODUCTION

From the twentieth-century to the present day, society has depended on energy sources for electricity, transportation, and economic growth. Energy sources are classified as chemical sources, thermal sources, electromagnetic radiation sources, mechanical sources, and nuclear sources.[1] Fossil fuels, such as coal, gas, oil, and tar, are chemical energy sources used in industries for various applications, such as transportation and electricity.[1] Crude oil, for example, is a chemical energy source refined into gasoline in petroleum industries and a source of energy for the transportation sector. Another chemical energy source is coal, which is used to create electricity to provide heating, cooling, and light to the public sector. These fossil fuels, however, are obtained from nature by extraction processes.

As of 2009, 81% of the world's commercial energy supply comes from fossil fuels.[1] According to the U.S. Energy Information Administration, which is part of the U.S. Department of Energy, demand for electricity will increase by 40% in the United States in the next 25 years.[2] However, the burning of fossil fuels in power plants results in greenhouse emissions[1,2] because flue gas exits the power plant and reaches the atmosphere afterward. Flue gas is a mixture of gases. Flue gas contains nitrogen (N_2),

---

This thesis follows the style of *The Journal of Physical Chemistry C*.

carbon dioxide (CO_2), water (H_2O), nitrogen oxides (NO_x), and sulfur oxides (SO_x), where nitrogen is mostly in the flue gas, while the rest of the gases have smaller compositions in the flue gas.[3, 4] Nonetheless, flue gas contains carbon dioxide, which is a greenhouse gas.[5] If flue gas is released to the atmosphere, carbon dioxide and toxic gases are emitted to the environment as well. Due to the coal and power plant activities in the early twentieth century until today, carbon dioxide concentrations in the atmosphere have increased from a concentration of 280 ppm to 360 ppm in 2002 and 385 ppm by 2009.[1,6]

To reduce carbon dioxide gas emissions from fossil fuel combustion activities, several technologies have been implemented in industries to sequester carbon dioxide and store carbon dioxide underground. Physical and chemical solvents, such as monoethanolamine (MEA), membranes, adsorption onto solids, and cryogenic separation are carbon sequestration methods used today.[5] New technologies are being explored to achieve low costs in carbon sequestration processes and improve carbon dioxide separation efficiency. Emerging technologies include metal- organic frameworks, membranes, carbonate-based systems, and ionic liquids.[5]

The purpose of this research project is to study the structures and physical properties of metal- organic framework porous solids and obtain adsorption selectivity factors for carbon dioxide in carbon dioxide and nitrogen mixtures, as well as carbon dioxide in carbon dioxide, nitrogen, and water mixtures at various temperatures in various MOFs.

In addition, the diffusion of carbon dioxide, water, and nitrogen in MOFs are investigated. The adsorbents studied in this research are Cu-BTC, MIL-47, and IRMOF-1, and the adsorbates studied in this project are carbon dioxide, water, and nitrogen. Lastly, this study mainly focuses on determining an eco-effective carbon sequestration method that will prevent global climate changes in the future by reducing greenhouse gas concentrations in the atmosphere that result from fossil fuel combustion processes.

Coal-fired power plants

To generate electricity from a coal-fired power plant, coal is first pulverized and fed into a boiler where the powdered coal is burned with air to generate heat and produce steam. The heat generated raises the temperature of water, causing the formation of steam. The steam passes through a turbine, labeled 8, to generate electricity, as shown in Figure 1.

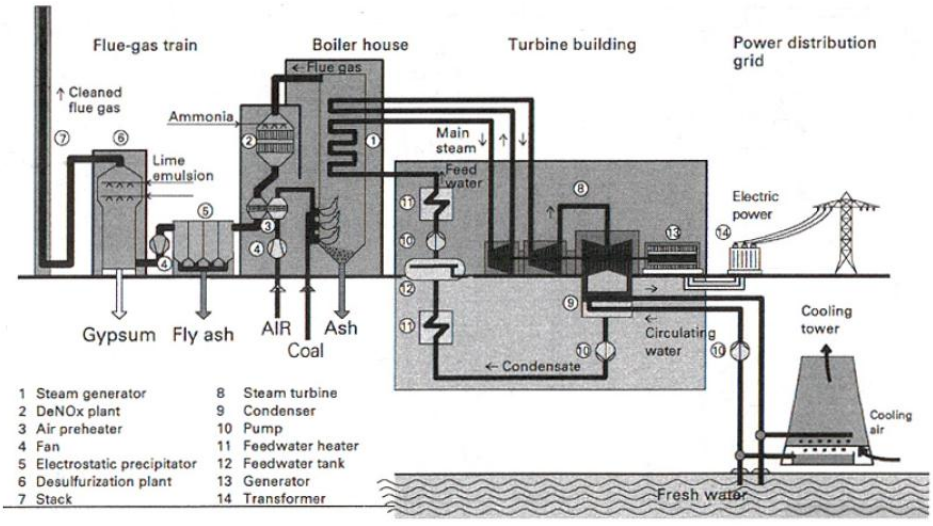

Figure 1. Coal-fired power plant.[7]

The steam turbine is connected to a generator, labeled 13. The generator is connected to a transformer, labeled 14, which provides electric power to the public sector. As seen in Figure 1, flue gas exits from the boiler house and enters a desulfurization plant. Afterward, cleaned flue gas exits the coal-fired power plant through a stack to the atmosphere. The cleaned flue gas contains carbon dioxide, nitrogen oxides, sulfur oxides, water, methane, oxygen, and nitrogen. The percent volume of carbon dioxide in flue gas is usually 13-15 vol% in coal-fired systems, and the pressure of the flue gas ranges from 100-175 kPa.[5] To sequester carbon dioxide, carbon dioxide is separated from the rest of the components in the flue gas. Once separation of carbon dioxide from the rest of the components is achieved, carbon dioxide is stored in tanks underground.

Carbon dioxide emissions

Carbon dioxide emissions in the United States have been increasing over the past 100 years. Figure 2 shows the amount of CO_2 released in the U.S. from 1800 to 2006.

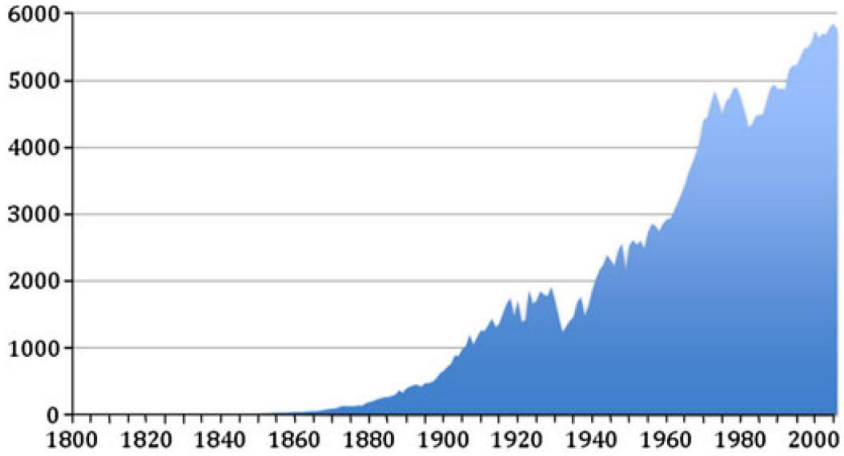

Figure 2. Carbon dioxide emissions in the United States.[8]

Carbon dioxide emissions come from different energy sectors. In Figure 3, two diagrams show energy consumption and greenhouse emissions for each energy sector.

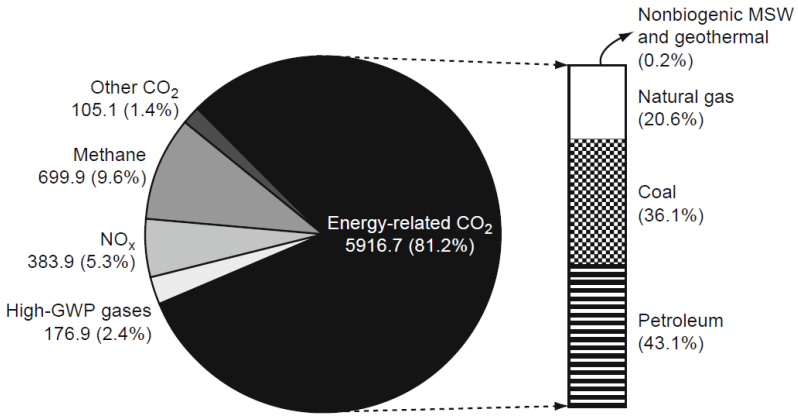

Figure 3. Carbon dioxide emissions from various energy sectors in the U.S.[5]

In 2007, the petroleum sector in the U.S. contributed the most in carbon dioxide emissions with 43.1%, while the coal sector emitted less carbon dioxide emissions compared to the petroleum sector. The coal sector contributed a total of 36.1% of the total carbon dioxide emissions in 2007. The rest energy sectors, which are nonbiogenic and geothermal and natural gas, emitted about 20.8% of the total carbon dioxide emissions in 2007. Based on the statistical data from the EIA, coal-fired power plants and petroleum industries release more carbon dioxide emissions to the environment in an annual basis. Because the atmosphere and the ozone layer do not have the capacity to accept all the carbon dioxide emissions produced from industrial activities, carbon dioxide emissions should be reduced and captured.[9]

Carbon dioxide sequestration technologies

As of today, technologies are used in industries to capture carbon dioxide from flue gas; however, many of these technologies are costly and do not efficiently separate carbon dioxide from flue gas. Physical and chemical solvents, such as monoethanolamine, membranes, adsorption onto solids, and cryogenic separation do not have the capacity to remove carbon dioxide from high-volume, low-CO_2 concentration flue gases due to high capital costs associated with installing post-combustion separation systems that will process a large volume of flue gas.[5] Post-combustion CO_2 capture has the ability to minimize carbon dioxide emissions because it can be integrated into power sector units that produce approximately 67% of the CO_2 emissions.[5]

Figure 4 shows a schematic of a post-combustion carbon dioxide capture system.

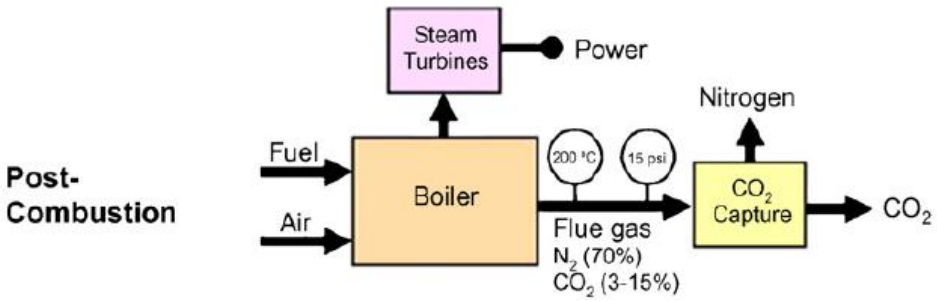

Figure 4. Post-combustion carbon dioxide capture system.[2]

Amine-based liquid solvent systems

In post-combustion capture systems where chemical solvents are implemented, the flue gas is cooled first and then enters the bottom of the absorber column.[5] The amine-based

liquid solvent enters the absorption column at the top.[5] MEA is commonly used to capture CO_2. In an amine-based liquid solvent system, the MEA, for instance, enters the absorber, while the flue gas enters the absorber from the bottom. Mass transfer occurs, and carbon dioxide is absorbed by MEA in counter-current flow. The carbon dioxide is separated from the flue gas and its components by chemical absorption, and carbon dioxide, along with the solvent, are collected by a heat exchanger.[5] As of now, the integration of amine-based liquid solvent in a post-combustion chemical absorption system has not been accomplished in industry to absorb 700 metric tons of carbon dioxide per hour for a 1000 MW_e plant because high energy consumption is required to absorb large quantities of carbon dioxide. In addition, the amine-based solvent may cause corrosion in the long term. Nevertheless, this carbon capture technology has the advantage of absorbing low-CO_2 partial pressure streams.[5] Figure 5 shows a diagram of a post-combustion capture plant where chemical absorption occurs

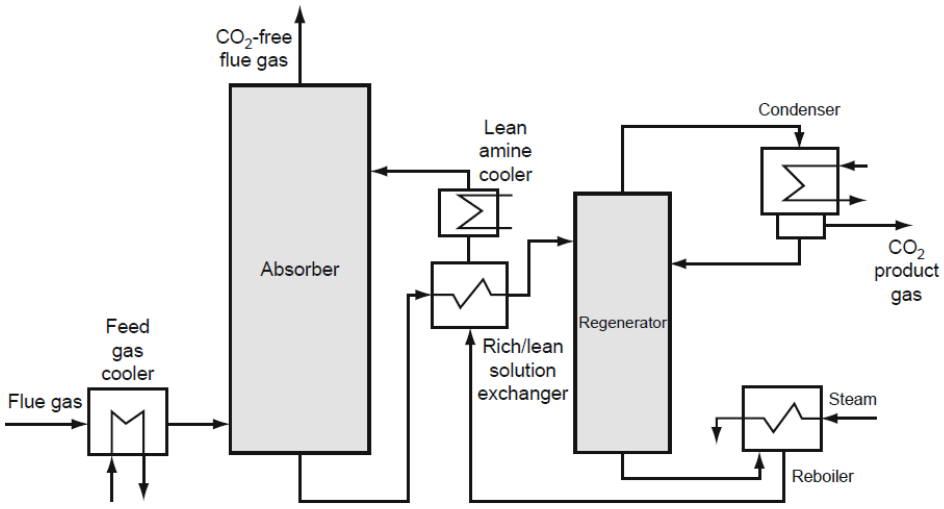

Figure 5. Post-combustion carbon dioxide capture with chemical absorption.[5]

Solid sorbents

Solid sorbents capture carbon dioxide via chemical absorption or physical adsorption. Solid sorbents are particles in the solid state that can separate carbon dioxide from flue gas streams through mass transfer in solid-gas phase. To absorb carbon dioxide in flue gas, solid particles and flue gas can be contacted by fluidized beds or fixed beds.[5]

Membranes

Membranes transport and separate carbon dioxide from flue gas through the use of permeable or semipermeable materials. The disadvantage of implementing membranes in post-combustion carbon dioxide capture systems is that membranes do not have the capacity to process large flue gas volumes and separate low carbon dioxide concentrations at low flue gas pressure. In addition, the surface area of the membranes is another factor that plays a role in separating carbon dioxide from flue gas. To effectively separate carbon dioxide from the rest of the components in the flue gas, membranes should have large surface area. The advantage of using membranes in post-combustion capture systems is basically that this gas-liquid phase membrane is able to stop cross-contamination and loss of absorption liquid.[5]

Ionic liquid systems

Ionic liquids contain an organic cation and an inorganic or organic anion. At room temperature, these ionic liquids are in liquid state. In addition, ionic liquids are nonvolatile and nonflammable. The advantage about ionic liquids is that these liquids

can dissolve carbon dioxide at various temperatures up to 100°C due to their stability. The other advantage about ionic liquids is that they are physical solvents that require little heat for regeneration. The major disadvantages of implementing ionic liquids in industry for carbon dioxide sequestration are high viscosity and costs.[5]

Metal-organic frameworks

Metal-organic frameworks are porous solids and materials that have inorganic nodes and organic compounds that are flexible under different temperature and pressure conditions.[10] These particular physical sorbents can be used to remove approximately ninety percent of carbon dioxide in flue gas streams.[10] A metal-organic framework is shown in Figure 6.

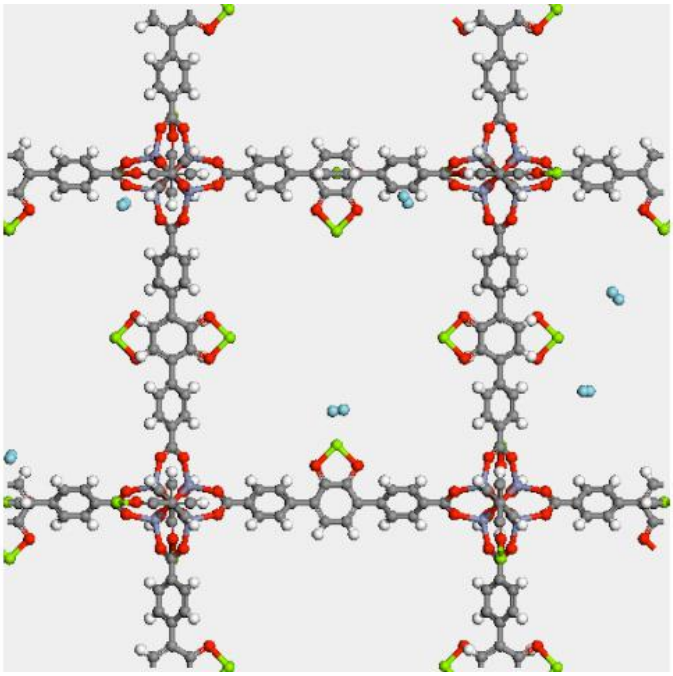

Figure 6. Schematic representation of IRMOF-16.[11]

Metal-organic frameworks can be rigid or flexible. Rigid MOFs have robust porous frameworks with permanent porosity. Flexible MOFs have soft frameworks that have an effect on pressure, temperature, and guest molecules. In MOFs, carbon dioxide, which is the adsorbate, is physically adsorbed and separated from the carrier gas depending on the physical interactions that take place between the metal sites in the MOF and the carbon dioxide.

Adsorption is the process where one or more components in a gas stream or a liquid stream are adsorbed onto the surface or the pores of a solid adsorbent.[12] Adsorption occurs in three steps. First, the component in the bulk gas, also known as the carrier gas, is transferred to the external surface of the adsorbent. Then, diffusion, which is transfer or movement of molecules through a fluid by random movements of the molecules, occurs, where the component molecule diffuses into the pores of the adsorbent. Lastly, the molecule adsorbs to the surface of the pore. In this study, adsorption and diffusion of carbon dioxide, water, and nitrogen are examined in three MOFs. The type of adsorption that occurs in MOFs is physical adsorption since the chemical nature of the adsorbate remains intact.[13] Metal-organic frameworks are formed by the synthesis of inorganic nodes and organic linker compounds. The inorganic nodes have metal ions or polynuclear metal clusters which are connected with organic ligands. The organic ligands are molecules that have carbon and hydrogen atoms.[10]

The synthesis of MOFs is shown in Figure 7.

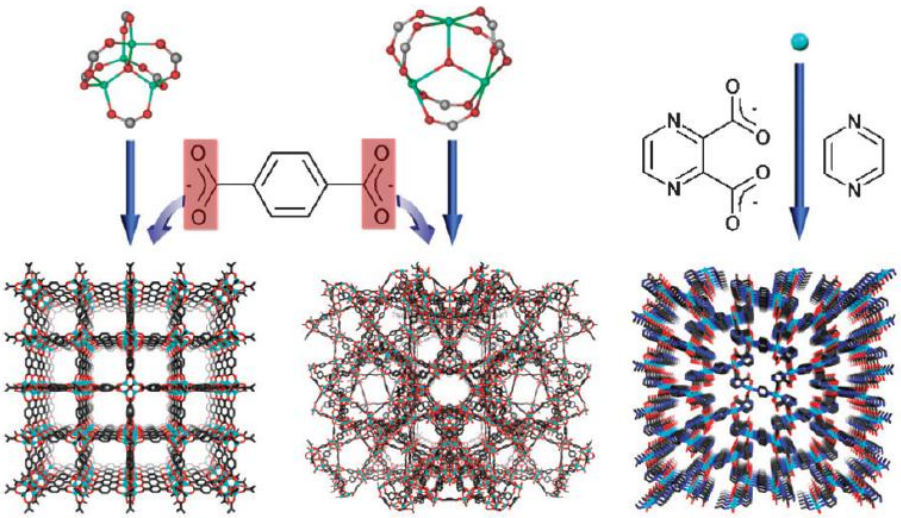

Figure 7. Synthesizing inorganic nodes and organic ligands.[10]

Metal-organic frameworks are materials that can be used for gas storage due to their large surface areas. Over the past ten years, more than 600 MOFs have been studied and synthesized by chemists and engineers. Recently, the U.S. Department of Energy (DOE) has requested a specific performance on sequestration and cost. To satisfy the specific performance on carbon dioxide sequestration, the MOF is required to have low energy requirement for regeneration, good thermal stability, tolerance to contaminants, and low cost.[2] The DOE requires 90% CO_2 capture at less than 35% increase in the cost of electricity.[6] Currently, adsorption and membrane processes, as well as absorption have not met the requirements set by DOE, but research still continues to determine the technology that will satisfy the conditions of the U.S. Department of Energy.

CHAPTER II

METHODS

Metal-organic framework models

To study the separation of carbon dioxide from water and nitrogen in flue gas streams, three metal-organic frameworks were selected. In this study, the selected metal-organic frameworks were Cu-BTC, IRMOF-1, and MIL-47. Cu-BTC, which has the chemical formula $Cu_3[(O_2C)_3C_6H_3]_2(H_2O)_3$, is composed of $Cu_2(COO)_4$ paddle wheels, copper dimers, and benzene-1,3,5-tricarboxylate (BTC).[14] IRMOF-1 has eight Zn_4O clusters linked by 24 linker molecules, which are 1,4-benzene dicarboxylates.[15] MIL-47, on the other hand, belongs to the MIL (Materials of the Institut Lavoisier) series and has the chemical formula $V(O)(O_2C\text{-}C_6H_4\text{-}CO_2)$.[14]

The crystal structure coordinates of each MOF were obtained from supporting information in literature.[16] To build the unit cells of Cu-BTC, IRMOF-1, and MIL-47 in Material Studio 5.5, structural properties and unit cell dimensions were obtained from Liu and Smit, as shown in Table 1, and used to construct the MOFs in Material Studio 5.5, which is a computer program that can change Cartesian coordinates into a 3-D model, measure bond angles, measure bond lengths, and calculate the charges of atoms in crystal structures.[14] In a $(1 \times 1 \times 1)$ unit cell, Cu-BTC has a total of 624 atoms. The unit cell of Cu-BTC has 48 copper atoms, 96 hydrogen atoms, 192 oxygen atoms, and 288 carbon atoms. On the other hand, IRMOF-1 has a total of 424 atoms in a $(1 \times 1 \times 1)$

unit cell. The unit cell of IRMOF-1 has 32 zinc atoms, 192 carbon atoms, 96 hydrogen atoms, and 104 oxygen atoms. MIL-47 has a total of 72 atoms in a (1 × 1 × 1) unit cell. The unit cell of MIL-47 has 4 vanadium atoms, 20 oxygen atoms, 32 carbon atoms, and 16 hydrogen atoms.

The Cartesian coordinates of carbon dioxide, nitrogen, and water were obtained from Material Studio 5.5. Nitrogen and carbon dioxide were built in Material Studio 5.5 as linear molecules. The Cartesian coordinates of carbon dioxide and nitrogen were used in Multipurpose Simulation Code[17-18] (MUSIC) program for GCMC simulations. The Cartesian coordinates of water were obtained from Atomistix ToolKit[19] and used in MUSIC program for GCMC simulations. For MD simulations, carbon dioxide, water, and nitrogen were added individually into the configuration of the MOFs using a Fortran 90 program. Table 1 provides geometry information for each MOF studied in this project, and Figures 8-10 illustrate the MOFs built in Material Studio 5.5.

Table 1: Unit Cell Geometry of IRMOF-1, Cu-BTC, and MIL-47

MOF	Unit Cell Dimensions (Å)	Cell Angle (Degree)
Cu-BTC	$a = b = c = 26.343$	$\alpha = \beta = \gamma = 90°$
MIL-47	$a = 6.818$, $b = 16.143$, $c = 13.939$	$\alpha = \beta = \gamma = 90°$
IRMOF-1	$a = b = c = 25.832$	$\alpha = \beta = \gamma = 90°$

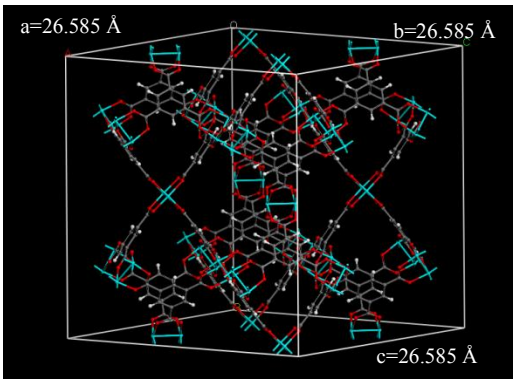

Figure 8. Cu-BTC (1 × 1 × 1) Unit Cell.

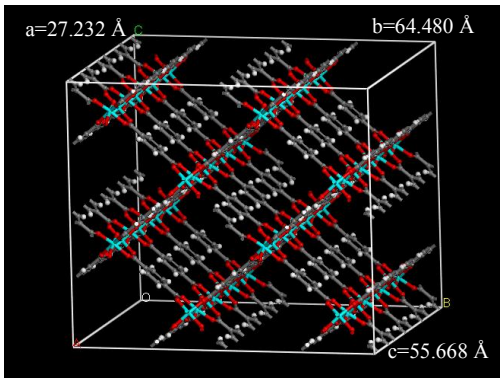

Figure 9. MIL-47 (4 × 4 × 4) Unit Cell.

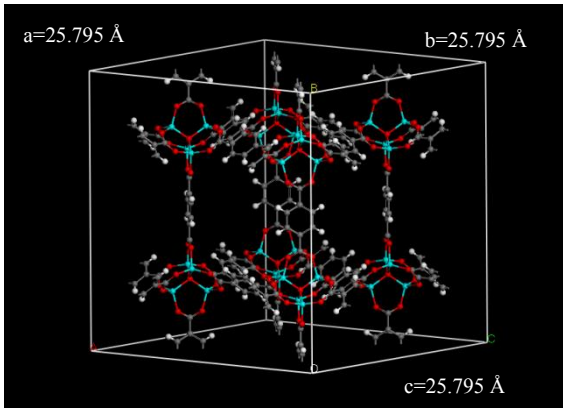

Figure 10. IRMOF-1 (1 × 1 × 1) Unit Cell.

Cu-BTC was selected because it is known to selectively adsorb carbon dioxide due to the strong interactions between copper and carbon dioxide. IRMOF-1 was chosen to study the adsorption of carbon dioxide in zinc metal. MIL-47 was also selected to determine if MIL series MOFs have high carbon dioxide selectivity. In addition, three MOFs were chosen to analyze the differences in selectivity and diffusion of carbon dioxide in MOFs that have a different metal site.

Forcefields

To account for the molecular interactions between adsorbates and adsorbents, Lennard Jones (LJ) potential parameters were used. The LJ potential model approximates the nuclear and electronic repulsions, as well as the electronic kinetic energy when molecules are close to each other and attractive forces dominate.[20] The term σ, which has units of length, is the "average collision diameter"[12], and the term ε, which has units of energy, is the depth of the potential well:

$$V(r) = 4\varepsilon\left\{\left(\frac{\sigma}{r}\right)^{12} - \left(\frac{\sigma}{r}\right)^{6}\right\} \quad (1)$$

The LJ potential parameters for the atoms in the selected metal-organic frameworks were obtained from the Dreiding force field.[21] The LJ parameters for the oxygen and carbon atoms in carbon dioxide, and the LJ parameters for the nitrogen atoms in nitrogen were taken from the transferable potentials for phase equilibria (TraPPE) force field model, which was developed by Potoff and Siepmann.[22] The LJ parameters for the oxygen and hydrogen atoms in water were taken from the simplified point charge (SPC/E) model developed by Berendsen, et. al.[23] To determine the LJ parameters between the atoms in the MOFs and the atoms in the adsorbates, the Lorentz-Berthelot mixing rules were applied.[24] The Lorentz-Berthelot mixing rules are shown in equation 2 and equation 3. These equations calculate the LJ potential parameters for the interaction of atomic pairs.

$$\sigma_{ij} = \frac{1}{2}(\sigma_{ii} + \sigma_{jj}) \quad (2)$$

$$\varepsilon_{ij} = (\varepsilon_{ii}\varepsilon_{jj})^{1/2} \quad (3)$$

The LJ parameters for the individual atoms in Cu-BTC, IRMOF-1, and MIL-47 are shown in Table 2. The LJ parameters of individual atoms in adsorbates for this study are shown in Table 3.

Table 2: **LJ Potential Parameters for the Atoms in IRMOF-1, Cu-BTC, and MIL-47**

Atom	σ (Å)	ε/v_B (K)
MOF_C	3.47	47.86
MOF_O	3.04	48.1
MOF_H	2.83	7.65
MOF_Cu	3.07	2.61
MOF_Zn	4.04	27.7
MOF_V	2.80	8.06
MOF_μ_2-O	3.04	48.1

Table 3: **LJ Potential Parameters for the Atoms in CO_2, N_2, and H_2O**

Atom	σ (Å)	ε/v_B (K)
C_CO_2	2.80	27.0
O_CO_2	3.05	79.0
N_N_2	3.31	36.0
H_H_2O	0.00	0.00
O_H_2O	3.16	80.0

In addition to LJ potential parameters, the charges of each atom in a metal-organic framework were assigned, and the overall net charge of the metal-organic framework was zero. The overall net charge of water, carbon dioxide, and nitrogen was also zero. The charges of the atoms in Cu-BTC and IRMOF-1 were obtained from supporting information in literature.[25] The charges of the atoms in MIL-47 were obtained from

Salles, et. al.[26] Nitrogen and carbon dioxide were modeled as rigid linear molecules, while water was model as a rigid non-linear molecule. The partial point charges of each atom site in nitrogen and carbon dioxide were also taken from the Trappe force field model developed by Potoff and Siepmann.[22] The partial point charge of +0.964*e* was assigned for the center of mass (COM) site in nitrogen, while a partial point charge of -0.482*e* was assigned for the nitrogen atoms. This model accounts for the quadrupole model of the N_2 molecule. Partial point charges centered at each LJ site in carbon dioxide were q_O = -0.35*e* and q_C = +0.70*e*. In this study, the partial point charges of water were taken from the SPC/E force field model.[23] Each water molecule was assigned a positive charge on the hydrogen atom (q_H =0.4238*e*) and a negative charge on the oxygen atom (q_{OW} = -0.8476*e*), thus yielding the dipole moment of the water molecule. Moreover, the charges of atoms in MOFs were assigned individually using Material Studio 5.5. MUSIC program was used to determine if the structures of Cu-BTC, IRMOF-1, and MIL-47 were neutrally charged. The charges of each atom in each metal-organic framework are shown in Tables 4, 5, and 6.

Table 4: **Charges of Atoms in Cu-BTC**

Atom	**Charge [e^-]**
H	+ 0.14
Ob	-0.59
Cu	+1.00
Carbon (Ca)	+0.68
Carbon (Cb)	-0.03
Carbon (Cc)	-0.11

Table 5: **Charges of Atoms in IRMOF-1**

Atom	Charge [e^-]
Zinc	+ 1.50
Oxygen (Oa)	-1.846
Oxygen (Ob)	-0.724
Carbon (Cb)	+0.072
Carbon (Ca)	+0.667
Carbon (Cc)	-0.132
Hydrogen (H)	+0.140

Table 6: Charges of Atoms in MIL-47

Atom	Charge [e^-]
H	+ 0.14
Ob	-0.499
V	+1.207
Carbon (Ca)	-0.071
Carbon (Cb)	0.60
Carbon (Cc)	-0.068
μ_2-O	-0.596

Computational simulation methods

Grand Canonical Monte Carlo simulations were implemented in this study to obtain the selectivity for CO_2 in CO_2/N_2 flue gas mixtures and the selectivity for CO_2 in $CO_2/N_2/H_2O$ flue gas mixtures at various temperatures. To perform GCMC simulations, Multipurpose Simulation Code (MUSIC) was used. MUSIC was developed by Gupta, et. al[17] in 2003 to study the adsorption isotherms of porous materials. In GCMC

simulations, each MOF was treated as a rigid molecule, and the Lorentz-Berthelot mixing rules were only applied between the atoms in the MOF and the adsorbates. In other words, the interactions between atoms in the MOF (adsorbent atom-adsorbent atom) were not considered in this study. The simulation boxes representing Cu-BTC and IRMOF-1contained 8 (2 × 2 × 2) unit cells, while the simulation box representing MIL-47 contained 16 (4 × 2 × 2) unit cells. For each GCMC simulation, the fugacity, which is the pressure of a real gas, of carbon dioxide, nitrogen, and water were specified. In this study, total pressures ranged from 100 kPa to 9000 kPa, while the temperatures ranged from 210 K to 323 K. Each GCMC simulation was set to 2×10^7 iterations and 2×10^6 steps.

The flue gas was particularly represented by carbon dioxide, nitrogen, and water molecules which were introduced at a particular temperature into the MOF. Various flue gas compositions were analyzed. The flue gas compositions selected were as follows: 85 mol% N_2-15 mol% CO_2, 85 mol% N_2-10 mol% CO_2-5 mol% H_2O, 90 mol% N_2-10 mol% CO_2, and 95 mol% N_2-5 mol% CO_2. These flue gas compositions were implemented in GCMC and MD simulations in order to study a representative flue gas composition. After the GCMC simulations were finished, the selectivity for CO_2 was obtained from the loading data provided by MUSIC program and the formula shown in equation 4, which accounts the composition of a component in a gas mixture and the amount adsorbed of a component.

$$S_{ads(i/j)} = \frac{x_i y_j}{x_j y_i} \tag{4}$$

The adsorption of carbon dioxide, nitrogen, and water in the metal-organic framework at various pressures and temperatures was observed using Visual Molecular Dynamics and Material Studio 5.5. The diffusion coefficients and the radial distribution functions were found using DL_POLY 2.20[27,28,29] software and Molecular Dynamics simulations, where the number of molecules, volume, and temperature remain constant (NVT). In MD simulations, the configuration of the flue gas was created using Fortran 90. The flue gas contained a total of 80 molecules in every computational experiment. The diffusion coefficients of carbon dioxide, nitrogen, and water in Cu-BTC, IRMOF-1, and MIL-47 were obtained by applying the mean-square displacement method and Albert Einstein diffusivity equation[26] shown below.

$$D_s(c) = \lim_{t\to\infty} \frac{1}{6t} \langle \frac{1}{N} \sum_{j=1}^{N} \left\| r_j(t) - r_o(0) \right\|^2 \rangle \quad (5)$$

The diffusivity equation has brackets,$\langle \dots \rangle$, which represents the ensemble average, and equation 5 also accounts for the vector position or movement of the molecules that diffuse in metal-organic frameworks by the function, r(t). The ensemble average is divided by *N*, which is the number of the molecules that diffuse in the system. The time step applied to all MD simulations for obtaining diffusion coefficients varied with the number of molecules in the system. If the number of molecules of carbon dioxide or water was smaller than eight molecules, a time step of 1×10^7 steps was used. The location and proximity of carbon dioxide, water, and nitrogen in MOFs was analyzed using radial distribution functions (RDF) until the MOF and the adsorbate molecules reached equilibrium at low temperatures and high temperatures. To acquire descriptive RDF graphs, the MD simulations consisted of 5×10^7 steps to guarantee equilibration.

CHAPTER III

RESULTS

Adsorption isotherms

The adsorption of water, carbon dioxide, and nitrogen in IRMOF-1, Cu-BTC, and MIL-47 were analyzed using GCMC simulations at various temperatures and low pressures. The amount of carbon dioxide and nitrogen adsorbed in Cu-BTC at 298 K for flue gas with a composition of 85 mol% N_2 and 15 mol% CO_2 is shown in Figure 11. The data was obtained using GCMC simulations and MUSIC program. Figure 11 illustrates Cu-BTC adsorbing more carbon dioxide than nitrogen at 298 K at low pressures and high pressures.

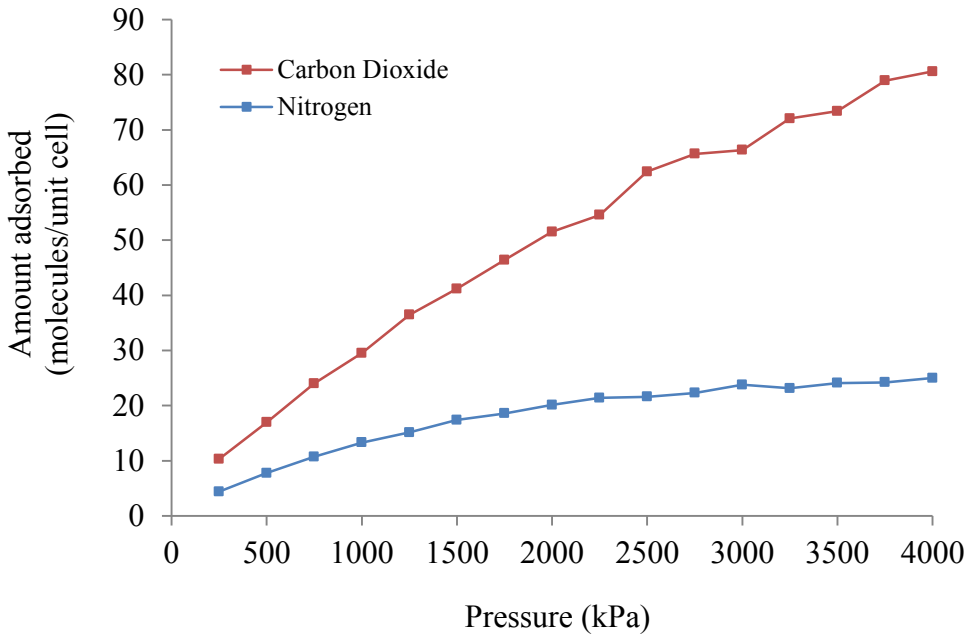

Figure 11. Amount adsorbed as a function of pressure for Cu-BTC and 85 mol% N_2 – 15 mol% CO_2 at 298 K.

The selectivity for CO_2 in a gas mixture is determined by using equation 4. A larger selectivity for carbon dioxide implies effective adsorption of carbon dioxide in MOFs. The data shown in Figure 12 is used to calculate the selectivity for CO_2. However, if the amount adsorbed of carbon dioxide is less than nitrogen for an 85 mol% N_2 and 15 mol% CO_2 mixture, then the selectivity would be low. For the flue gas with a composition of 85 mol% N_2 and 15 mol% CO_2 at 298 K, the selectivity for CO_2 increases as pressure increases because the amount of carbon dioxide adsorbed by Cu-BTC increases with pressure.

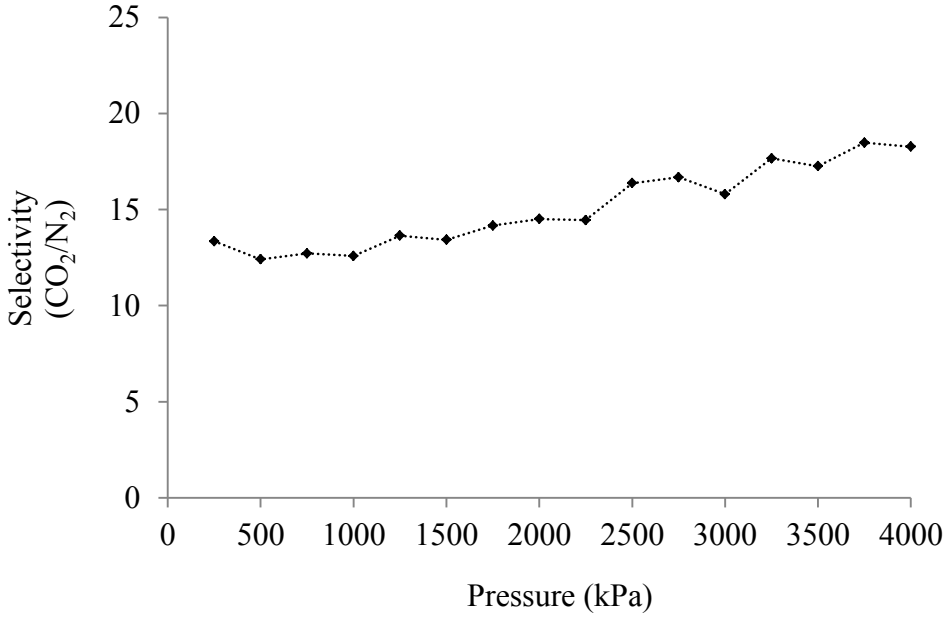

Figure 12. Selectivity as a function of pressure for Cu-BTC and 85 mol% N_2 –15 mol% CO_2 at 298K.

In Figure 13, two illustrations of the Cu-BTC system are shown. The illustrations were obtained using Material Studio 5.5. Figure 13-a shows the initial configuration of Cu-BTC before carbon dioxide and nitrogen enter and interact with the system. Figure 13-b displays Cu-BTC and flue gas adsorption. Figure 13-b shows adsorption of carbon dioxide and nitrogen. At 298 K, carbon dioxide and nitrogen are adsorbed by copper metal sites. In addition, the highest pressure at which the flue gas is adsorbed in Cu-BTC is 4000 kPa. Figure 8, shown earlier, represents one cubic unit cell, whereas Figure 13 shows the front profile of a $2 \times 2 \times 2$ unit cell.

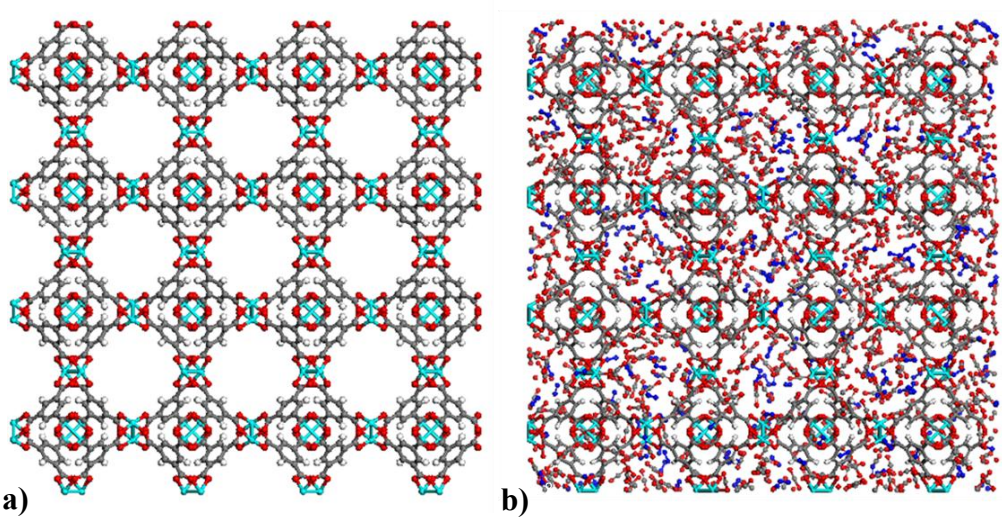

Figure 13. (a) The initial configuration of Cu-BTC at 298K and 0 kPa. (b) final configuration of Cu-BTC at 298 K and 4000 kPa and adsorption of flue gas with a composition of 85 mol% N_2 and 15 mol%. Copper atoms are represented in cyan. Hydrogen atoms are represented in white; carbon atoms are shown in gray; oxygen atoms are illustrated in red; nitrogen atoms are shown in blue.

To determine the temperature effect on the selectivity for CO_2 for a gas mixture that consists of 85 mol% N_2 and 15 mol% CO_2, adsorption isotherms were obtained using MUSIC program and GCMC simulations at various temperatures and three constant pressures. The constant pressures are 1000 kPa, 2000 kPa, and 4000 kPa. Table 7 shows selectivity for CO_2 increasing as pressure increases; thus, copper metal in Cu-BTC effectively adsorbs and strongly interacts with carbon dioxide at higher pressures.

Table 7: Cu-BTC Selectivity for CO_2 in Flue Gas with a Composition of 85 mol% N_2 and 15 mol% CO_2 at Constant Pressures and Low and High Temperature Conditions

	P = 1000 kPa	**P = 2000 kPa**	**P = 4000 kPa**
Temperature (K)	Selectivity (CO_2/N_2)	Selectivity (CO_2/N_2)	Selectivity (CO_2/N_2)
170	8.758	13.134	17.101
190	14.685	30.647	46.379
230	139.654	217.999	238.873
273	21.594	30.019	44.218
298	12.627	14.207	18.730
313	10.407	11.125	13.709

To analyze the effect of temperature on selectivity for carbon dioxide, the data in Table 7 is plotted in an x-y axis graph. The behavior of selectivity for CO_2 in CO_2/N_2 mixtures as temperatures increases is non-linear. Figure 14 shows selectivity having a maximum at 210 K for three different pressures and also illustrates selectivity decreasing at higher temperatures. The copper-metal in Cu-BTC strongly interacts with carbon dioxide at low temperatures and high pressures. On the other hand, when the temperature is higher than room temperature, the carbon dioxide moves at high velocities; as a result, the carbon dioxide does not attach to the copper-metal easily.

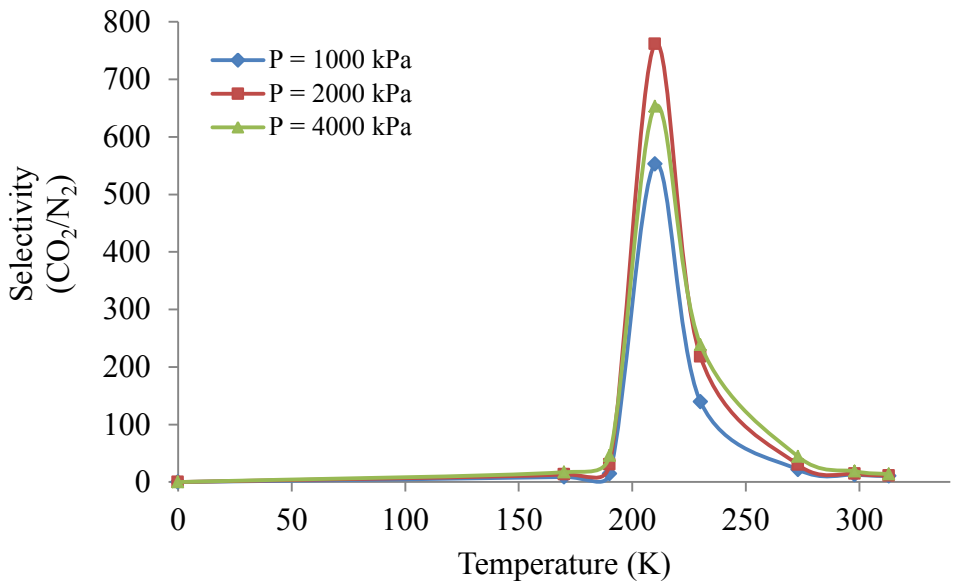

Figure 14. Selectivity as a function of temperature for a 85 mol% N2 –15 mol% CO2 gas mixture in Cu-BTC at 298K.

Figure 14 illustrates selectivity increasing after a temperature of 170 K. The selectivity for CO_2 increases rapidly after 190K and reaches a maximum at 210 K. After 210K, however, the selectivity for CO_2 in Cu-BTC decreases at higher temperatures. The adsorption of carbon dioxide is highest at a temperature of 210 K. At 210 K, the copper metal and the carbon dioxide interact strongly at the intermolecular level.

A ternary gas mixture was also simulated in MUSIC. The composition of the ternary system was 5 mol% H_2O, 10 mol% CO_2, and 85 mol% N_2. The flue gas was adsorbed in Cu-BTC at 298 K and pressures up to 4000 kPa. Based on Figure 15, water strongly adsorbs in Cu-BTC at 298 K, whereas nitrogen and carbon dioxide are weakly adsorbed. The amount of water adsorbed increases with pressure, whereas the amount of carbon dioxide and nitrogen increase with pressure but decrease after 1500 kPa.

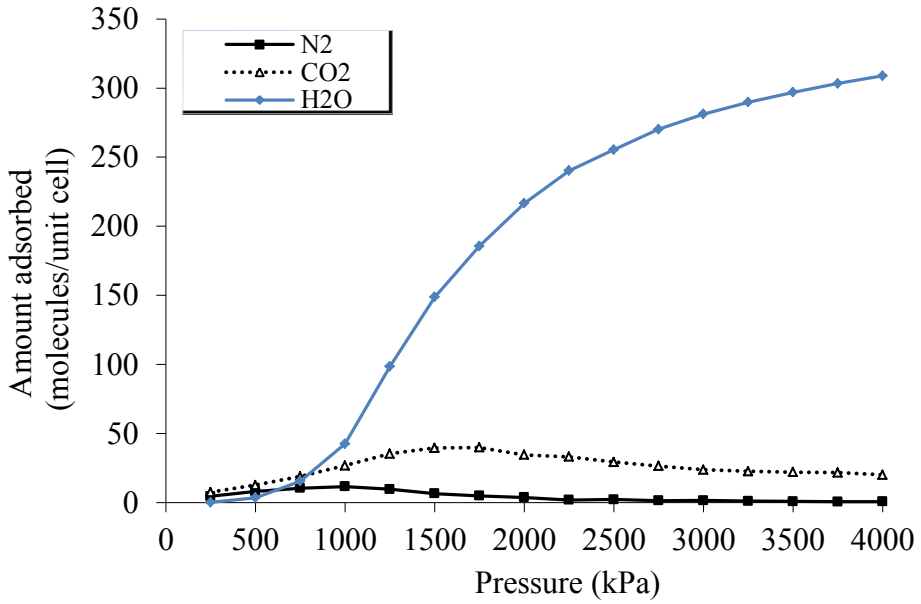

Figure 15. Amount adsorbed as a function of pressure for a 5 mol% H_2O/10 mol% CO_2/85 mol% N_2 flue gas at 298 K.

For the flue gas with a composition of 85 mol% N_2, 10 mol% CO_2, and 5 mol% H_2O at 298 K, the Cu-BTC selectivity for CO_2 does not increase with pressure. At certain pressures, such as 3000 kPa, the selectivity decreases and increases after 3000 kPa. From Figure 16, we can see that the selectivity for carbon dioxide is higher when water is present in the flue gas mixture.

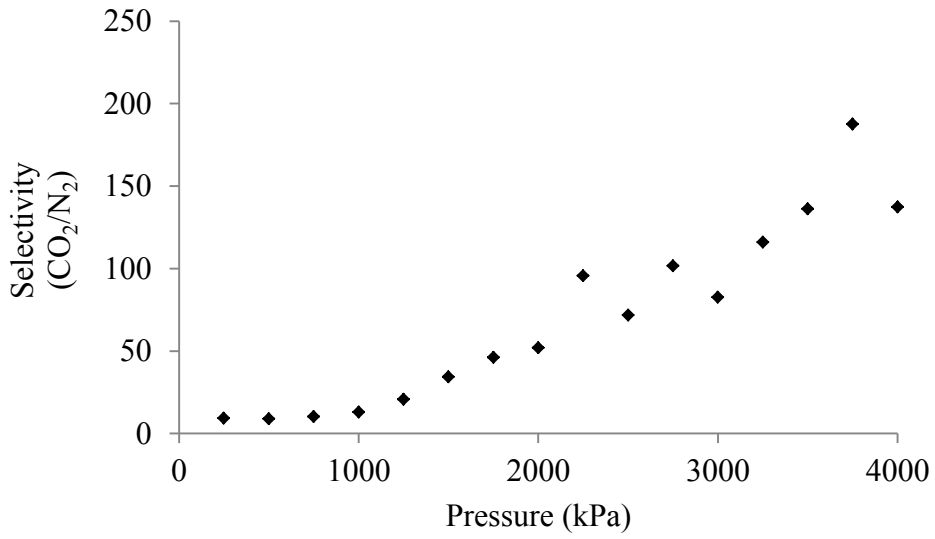

Figure 16. Selectivity as a function of pressure for a 5 mol% H_2O/10 mol% CO_2/85 mol% N_2 flue gas in Cu-BTC at 298K.

Figure 17 shows adsorption of water in Cu-BTC at 298 K. The carbon dioxide molecules are shown as linear molecules, and the water molecules are non-linear molecules. To determine the distance of water away from the copper metal sites, radial distribution functions were obtained for further analysis.

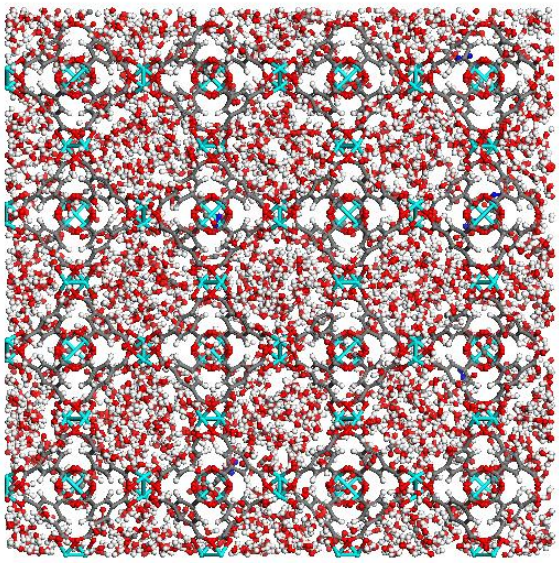

Figure 17. Snapshot of water adsorption in Cu-BTC at 298K. Copper atoms are represented in cyan. Hydrogen atoms are represented in white; carbon atoms are shown in gray; oxygen atoms are illustrated in red.

The amount of carbon dioxide and nitrogen adsorbed in IRMOF-1 at 298 K for flue gas with a composition of 85 mol% N_2 and 15 mol% CO_2 is shown in Figure 18. The data was obtained using GCMC simulations. Figure 18 illustrates the amount adsorbed for carbon dioxide and nitrogen increasing as pressure increases. Carbon dioxide is also more strongly adsorbed than nitrogen at 298 K at higher pressures but is less strongly adsorbed in IRMOF-1 than nitrogen at lower pressures.

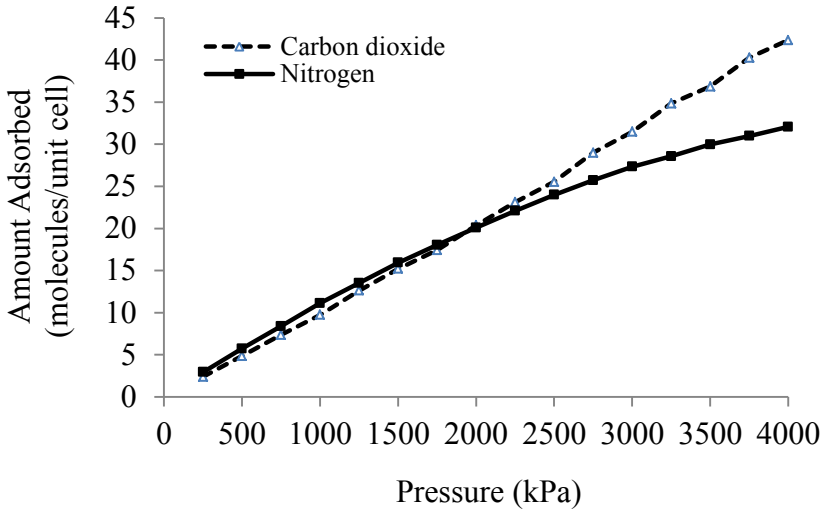

Figure 18. Amount adsorbed as a function of pressure for 15 mol% CO_2 – 85 mol% N_2 flue gas at 298 K in IRMOF-1.

The selectivity was calculated for the flue gas with a composition of 85 mol% N_2 and 15 mol% CO_2. The IRMOF-1 selectivity for CO_2 increases as pressure increases. Based on Figure 19, we can conclude that the IRMOF-1 selectivity for CO_2 is lower than Cu-BTC selectivity for carbon dioxide at 298 K.

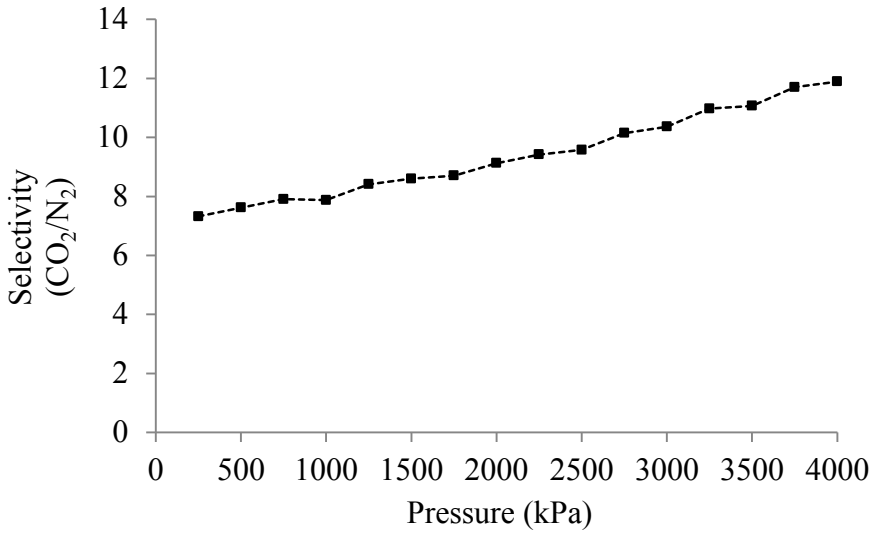

Figure 19. Selectivity as a function of pressure for 85 mol% N2 – 15 mol% CO_2 flue gas in IRMOF-1 at 298K.

To visualize the adsorption of carbon dioxide and nitrogen in IRMOF-1, Material Studio 5.5 program was used. The initial structure of IRMOF-1 is shown in Figure 20-a, and the final structure of IRMOF-1 after adsorption occurred is shown in Figure 20-b. Figure 20-b shows less N_2 and CO_2 molecules adsorbed in IRMOF-1 at 4000 kPa at 298 K for a flue gas with composition of 85 mol% N_2 and 15 mol% CO_2 when compared to Cu-BTC adsorption. The adsorption of carbon dioxide and nitrogen in Cu-BTC was higher because the copper atoms in Cu-BTC strongly interact with CO_2 at low and high pressures. The loading data can be confirmed using visualization programs, such as VMD or Material Studio 5.5. Figure 12-b confirms less adsorption of CO_2 and N_2 in IRMOF-1 at 298 K and 4000 kPa.

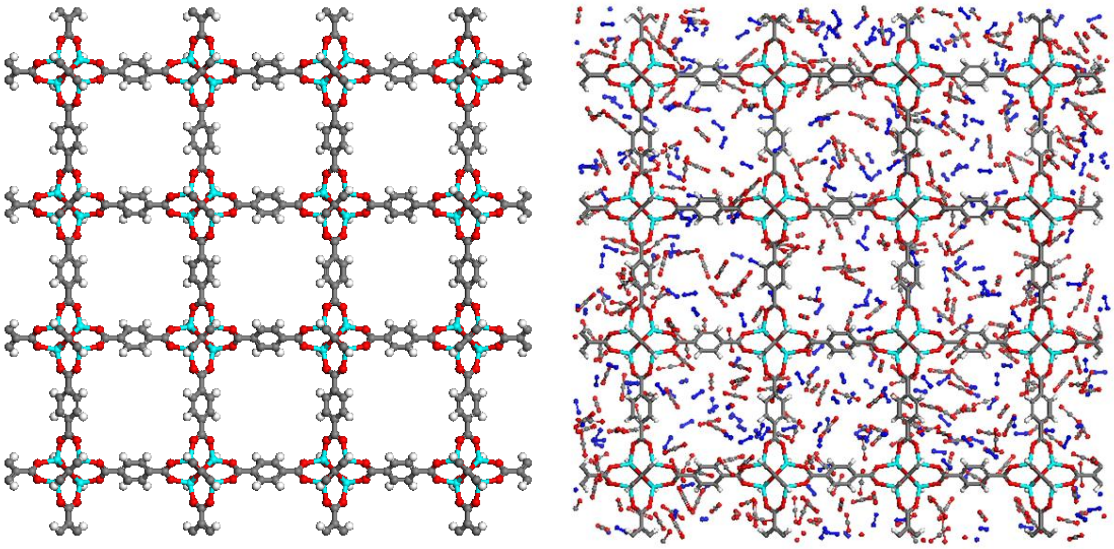

Figure 20. (a) The initial configuration of IRMOF-1 at 298K and 0 kPa. (b) final configuration of IRMOF-1 at 298 K and 4000 kPa and adsorption of flue gas with a composition of 85 mol% N_2 and 15 mol% CO_2. Zinc atoms are represented in cyan. Hydrogen atoms are represented in white; carbon atoms are shown in gray; oxygen atoms are illustrated in red; nitrogen atoms are shown in blue.

To analyze the selectivity for CO_2 in a gas mixture at various temperatures and constant pressures in IRMOF-1, GCMC simulations were performed for a flue gas with a composition of 85 mol% N_2 and 15 mol% CO_2. Simulations were run for a period of 1×10^7 steps. Table 8 and Figure 21 were obtained after calculating the selectivity for CO_2.

Table 8: IRMOF-1 Selectivity for CO_2 in Flue Gas with a Composition of 85 mol% N_2 and 15 mol% at Constant Pressures and Low and High Temperature Conditions

	P = 1000 kPa	**P = 2000 kPa**	**P = 4000 kPa**
Temperature (K)	Selectivity (CO_2/N_2)	Selectivity (CO_2/N_2)	Selectivity (CO_2/N_2)
170	56.3670	61.183	78.139
190	157.464	197.073	261.956
200	161.225	204.161	305.973
230	62.094	110.145	124.466
273	11.648	14.394	26.991
298	7.873	9.126	11.890
303	7.601	8.594	10.919
323	3.950	4.297	4.891

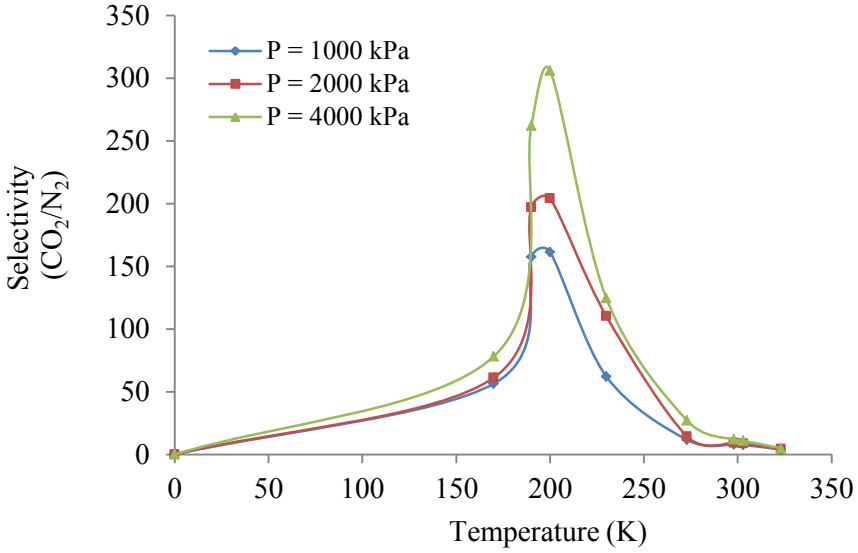

Figure 21. Selectivity as a function of temperature for 85 mol% N_2 – 15 mol% CO_2 flue gas in IRMOF-1 at 298K.

Figure 21 shows the selectivity for CO_2 increasing as pressure increases. IRMOF-1 also interacted strongly with carbon dioxide at low temperatures, but at room temperature, the selectivity was lower than 210 K. Figure 21 shows selectivity reaching a maximum at 200 K. As pressures increases at 200 K, the selectivity increases. Carbon dioxide is strongly adsorbed to the zinc metal in IRMOF-1 at 200 K and 4000 kPa.

GCMC simulations were performed for a flue gas with a composition of 5 mol% H_2O, 10 mol% CO_2 and 85 mol% N_2 at 298 K and to a maximum pressure of 4000 kPa for a period of 2×10^7 steps. The flue gas was adsorbed in IRMOF-1 at 298 K. To determine the difference in amount adsorbed for each component in the flue gas, adsorption

isotherms were constructed. Figure 22 shows significant water adsorption in IRMOF-1. In addition, Figure 22 shows a constant amount of water adsorbed between 3000 kPa and 4000 kPa. On the other hand, Figure 22 shows low carbon dioxide and nitrogen adsorption at all pressures because the zinc and the water molecules are strongly interacting at the temperature conditions and pressures set in GCMC simulations.

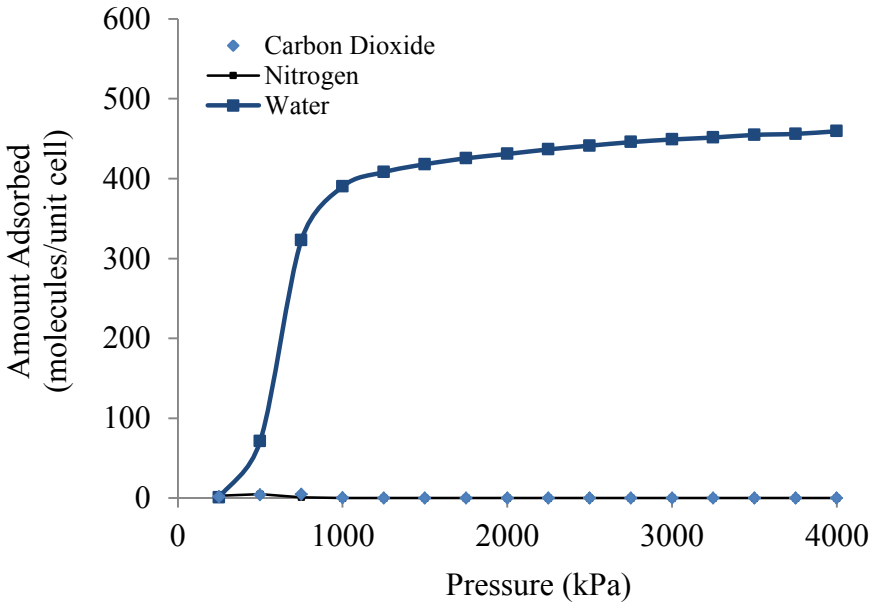

Figure 22. Amount adsorbed as a function of pressure for 5 mol% H_2O/10 mol% CO_2/85 mol% N_2 flue gas at 298 K in IRMOF-1.

The selectivity for CO_2 in a gas mixture with a composition of 5 mol% H_2O, 10 mol% CO_2, and 85 mol% N_2 in IRMOF-1 at 298 K was calculated using equation 4 and the amount adsorbed data from GCMC simulations and MUSIC program. The results are shown in Figure 23. For this particular case, the selectivity for CO_2 did not show a linear behavior as pressure increased because we can see that the selectivity does not constantly increase or decrease as pressure increases in the system.

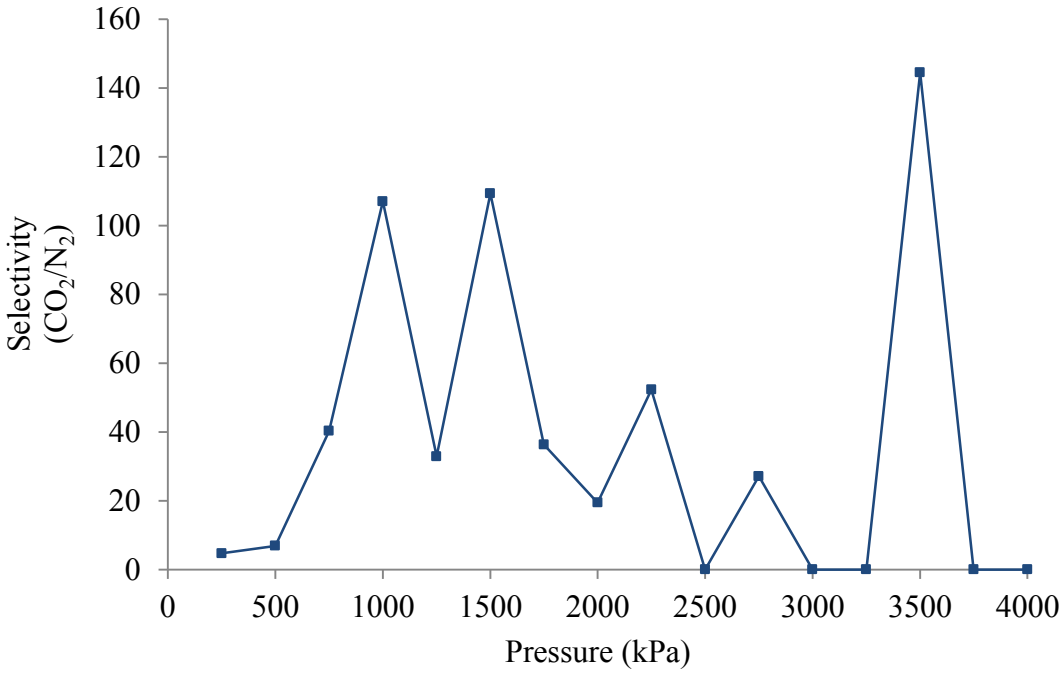

Figure 23. Selectivity as a function of pressure for 85 mol% N_2/10 mol% CO_2/5 mol% H_2O flue gas in IRMOF-1 at 298K.

MIL-47 was analyzed in MUSIC, and GCMC simulations were performed to determine the selectivity for CO_2 at 298 K and various temperatures. Furthermore, water adsorption was also analyzed to determine if the MOF strongly adsorbs water at room temperature. First, a flue gas with a composition of 85 mol% N_2 and 15 mol% CO_2 was simulated using MUSIC program and GCMC simulations were performed for MIL-47 at for a maximum pressure of 4000 kPa and a temperature of 298 K. The carbon dioxide and nitrogen adsorbed at 298 K are shown in Figure 24, which shows a higher amount of adsorption for carbon dioxide compared to nitrogen. In addition, the amount adsorbed for both species increases as pressure increases.

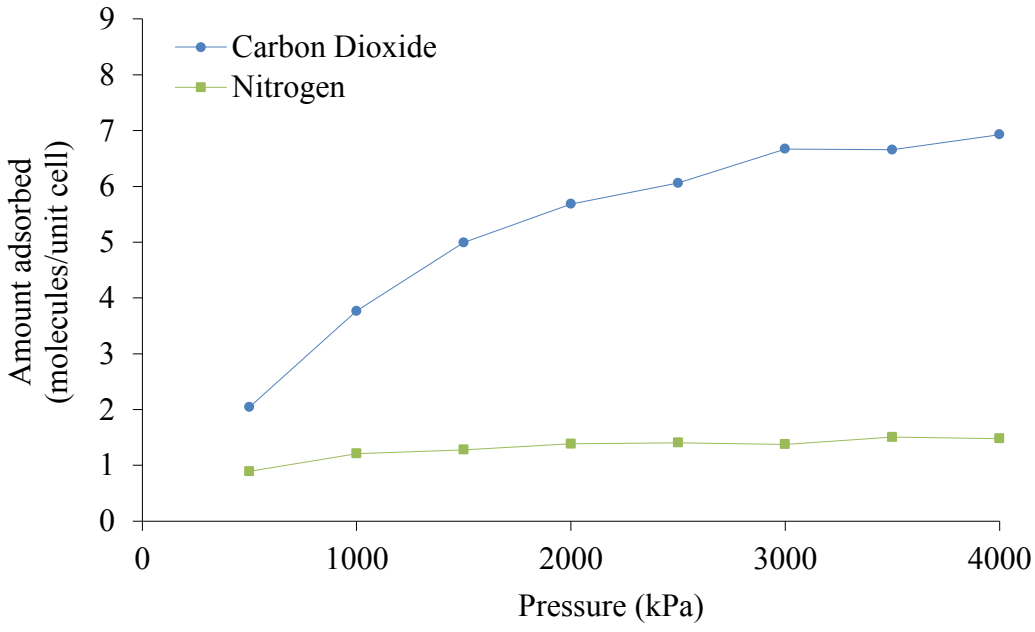

Figure 24. Amount adsorbed as a function of pressure for 15 mol% CO_2 – 85 mol% N_2 flue gas at 298 K in MIL-47.

The selectivity for CO_2 was determined by using equation 4. The selectivity for CO_2 for MIL-47 varying as a function of pressure is shown in Figure 25 for a flue gas with a composition of 85 mol% N_2 and 15 mol% CO_2 at 298 K. Based on Figure 25, selectivity for CO_2 initially increases as pressure increases; however, the selectivity varies as pressures get higher. For instance, the selectivity decreases at 3500 kPa and increases at 4000 kPa. Figure 25 also confirms that MIL-47 has a higher selectivity for CO_2 at 298 K for a flue gas with a composition of 85 mol% N_2 and 15 mol% CO_2 compared to IRMOF-1 and Cu-BTC.

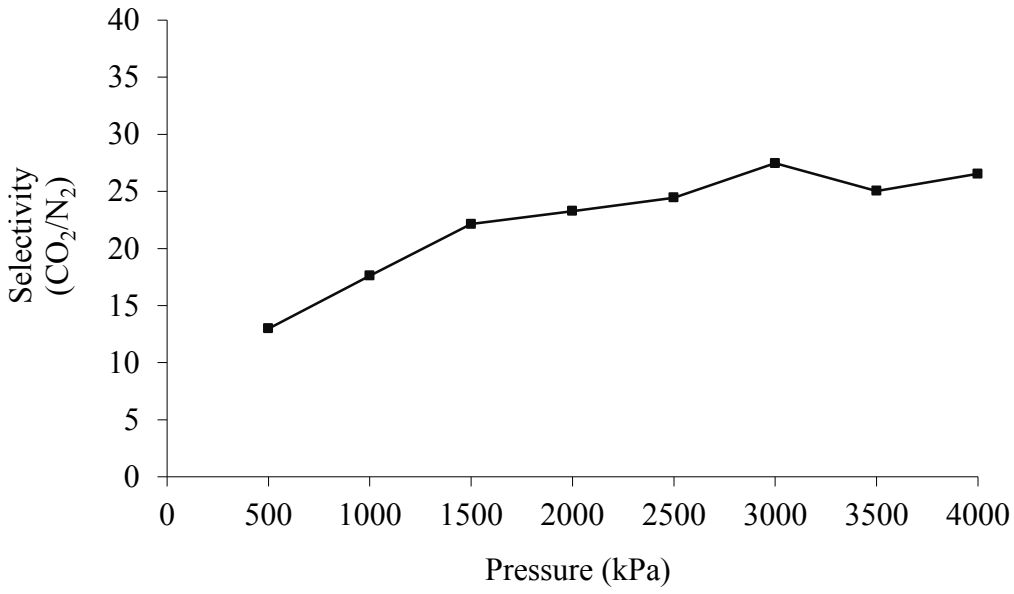

Figure 25. Selectivity as a function of temperature for 85 mol% N_2 – 15 mol% CO_2 flue gas in MIL-47 at 298K.

To visualize the adsorption of carbon dioxide and nitrogen in MIL-47, Material Studio 5.5 was used. The initial configuration of MIL-47 at 4000 kPa was visualized in Material Studio 5.5, which is shown in Figure 26-a. Figure 26-b shows carbon dioxide molecules and nitrogen molecules confined in the MIL-47 structure at room temperature and adsorption taking place. In addition, Figure 26-a shows the unit cell of MIL-47, which has orthorhombic boundary conditions.

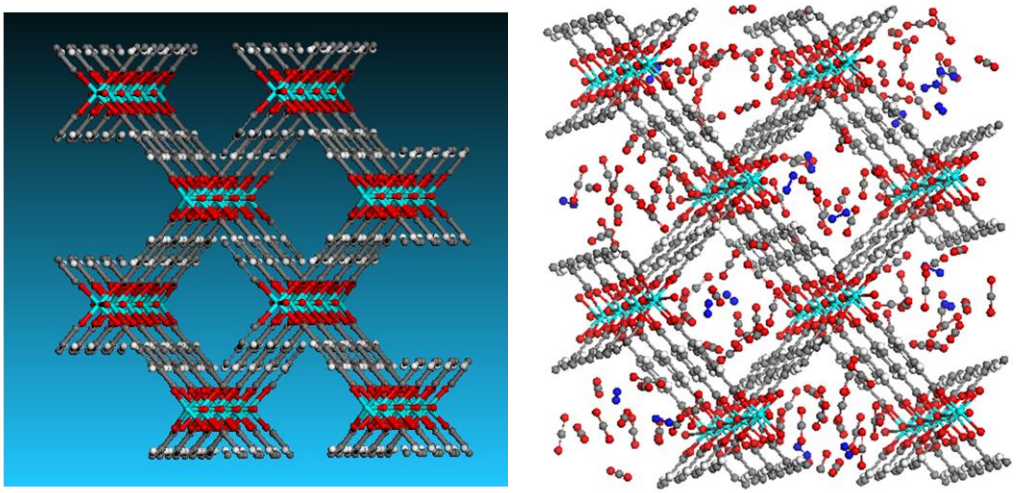

Figure 26. (a) The initial configuration of MIL-47 at 298K and 0 kPa. (b) final configuration of MIL-47 at 298 K and 4000 kPa and adsorption of flue gas with a composition of 85 mol% N_2 and 15 mol%. Vanadium atoms are represented in cyan. Hydrogen atoms are represented in white; carbon atoms are shown in gray; oxygen atoms are illustrated in red; nitrogen atoms are shown in blue.

The selectivity for CO_2 in MIL-47 was measured at different temperatures to determine the maximum selectivity at a particular temperature using GCMC simulations. The computational results are shown in Table 9. The results were also plotted in an x-y axis as shown in Figure 27, where we can observe selectivity for CO_2 increasing initially at low temperatures and then decreasing at higher temperatures.

Table 9: MIL-47 Selectivity for CO_2 in Flue Gas with a Composition of 85 mol% N_2 and 15 mol% at Constant Pressures and Low and High Temperature Conditions

	P = 1000 kPa	**P = 2000 kPa**	**P = 4000 kPa**
Temperature (K)	Selectivity (CO_2/N_2)	Selectivity (CO_2/N_2)	Selectivity (CO_2/N_2)
0	0	0	0
140	10.95	12.87	14.50
170	159.31	196.11	362.96
200	572.04	701.67	2204.00
240	136.85	130.74	252.57
273	43.60	51.83	59.17
298	19.85	24.75	30.60
323	10.63	11.85	16.20

Furthermore, the selectivity for CO_2 in MIL-47 reached a maximum at a temperature of 200 K. Based on Figure 14, 21, and 27, we can conclude that the selectivity for CO_2 in the three MOFs had a maximum in the range of 200-220 K where the gas molecules were not at a high kinetic energy state or at a low kinetic energy state.

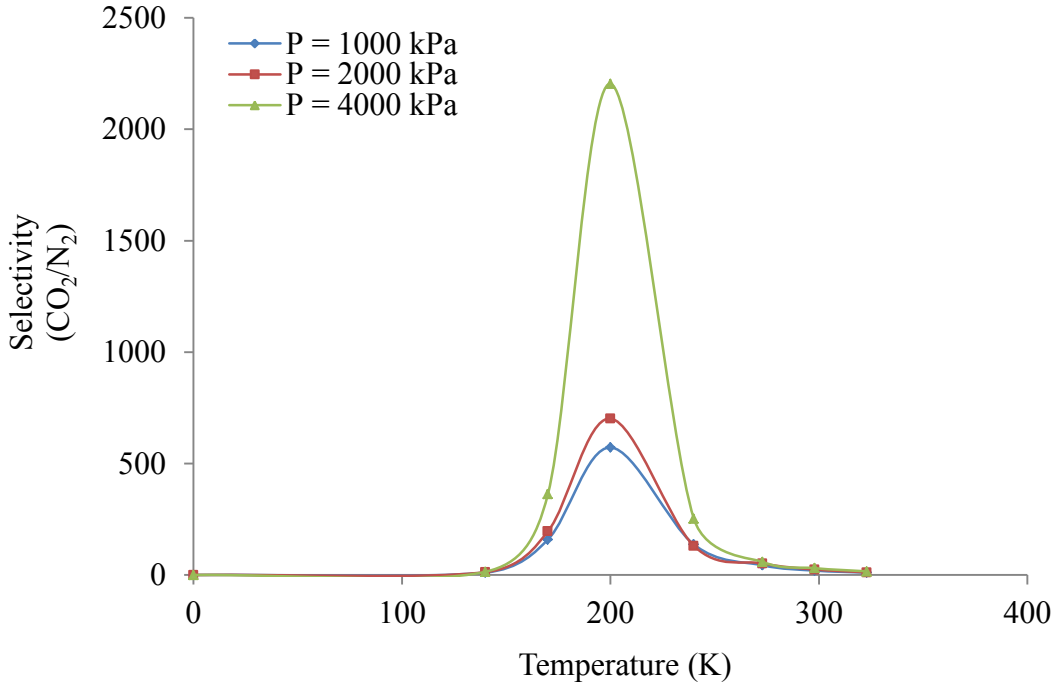

Figure 27. Selectivity as a function of temperature for 85 mol% N_2 – 15 mol% CO_2 flue gas in MIL-47 at 298K.

The adsorption of flue gas with a composition of 5 mol% H_2O, 10 mol% CO_2, and 85 mol% N_2 was simulated at 298 K in MIL-47 using GCMC simulations and MUSIC program. The adsorption isotherms of CO_2, H_2O, and N_2 were obtained at 298 K after 1×10^7 steps. Figure 28 shows water adsorption reaching a constant value of 25 molecules per unit cell at 3000 kPa and higher pressures. However, the amount of carbon dioxide and nitrogen adsorbed in MIL-47 was 0 molecules per unit cell. Water was mostly adsorbed in MIL-47 because water has a higher affinity to the vanadium metal sites in MIL-47, whereas carbon dioxide and nitrogen competed with water molecules for the same vanadium active sites.

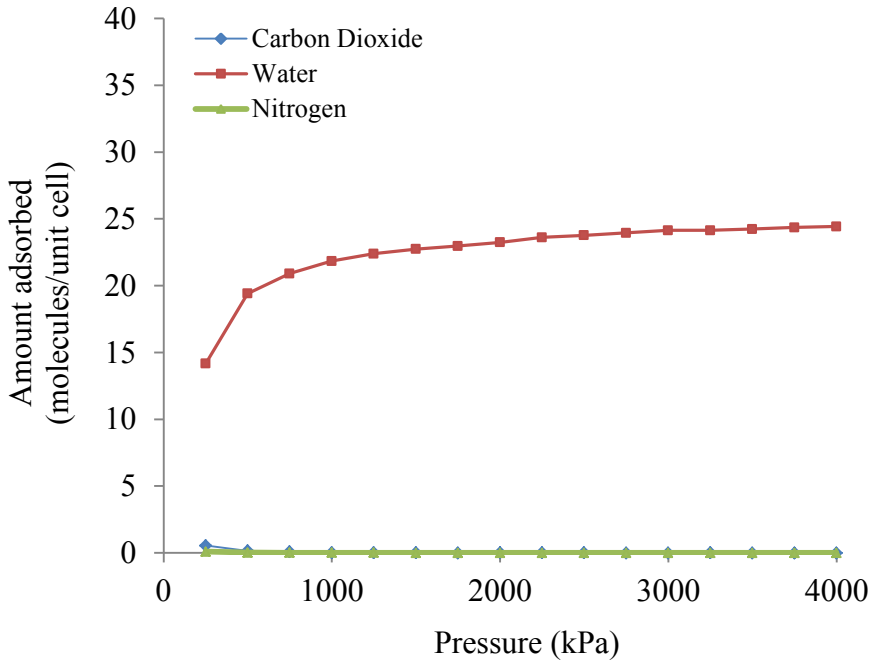

Figure 28. Amount adsorbed as a function of pressure for 5 mol% H_2O/10 mol% CO_2/85 mol% N_2 flue gas at 298 K in MIL-47.

Diffusion coefficients

To study the movement of carbon dioxide, water, and nitrogen in the MOF, the diffusion coefficient of each component in the flue gas was obtained using MD simulations, DL_POLY software, and the mean-square displacement method after a simulation period of 100 ps. Figure 29 shows the mean-square displacement as a function of time for N_2. The slope of the mean-square displacement function was used to calculate the diffusion coefficient. The slope of the line shown in Figure 29 is the average of the distance that the particle traveled during the time period of simulation divided by the number of molecules for that particular species. To determine the diffusion coefficient, the slope was multiplied by one-sixth, which is shown in equation 5. The mean-square displacement as a function of time is obtained using Fortran 90 program.

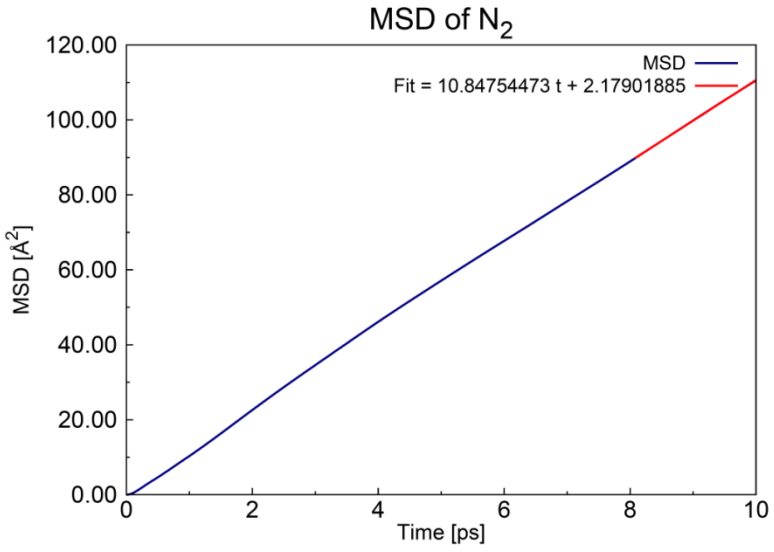

Figure 29. Mean-square displacement of N_2 as a function of time.

The diffusion coefficients of carbon dioxide, nitrogen, and water varied at different temperatures in MOFs and compositions. Table 10 provides information about the diffusion coefficients of carbon dioxide and nitrogen in binary gas mixtures and ternary gas mixtures with a total number of 80 gas molecules in IRMOF-1. Based on the MD and mean-square displacement data shown in Table 10, eighty nitrogen molecules diffused faster (D_s = 0.000314 cm^2/s) than eighty carbon dioxide molecules (D_s = 0.000128 cm^2/s) in IRMOF-1 at 298 K. Furthermore, an equimolar mixture of carbon dioxide and nitrogen at 298 K that has a total of eighty gas molecules was also analyzed in IRMOF-1. For an equimolar mixture with a total of eighty molecules, Carbon dioxide diffused at a slower rate than nitrogen. Carbon dioxide does not diffuse as fast as nitrogen because a quadrupole moment is present in carbon dioxide that allows carbon dioxide to attach strongly and interact with zinc metal sites in IRMOF-1.

Table 10: Diffusion Coefficients of Carbon Dioxide, Nitrogen, and Water in IRMOF-1 at 298K for a System of 80 Molecules

Carbon Dioxide		Nitrogen		Water	
Percent (%)	D_s (cm^2/s)	Percent (%)	D_s (cm^2/s)	Percent (%)	D_s (cm^2/s)
0	N/A	100	0.0003140	0	N/A
5	0.0000903	95	0.0003050	0	N/A
5	0.0001560	85	0.0003320	10	0.00008916
10	0.0000953	85	0.0003550	5	0.00019700
10	0.0000413	90	0.0002949	0	N/A
15	0.0001200	85	0.0002950	0	N/A
50	0.0001500	50	0.0002785	0	N/A
100	0.0001280	0	N/A	0	N/A

Table 11: Diffusion Coefficients of Carbon Dioxide, Nitrogen, and Water in IRMOF-1 at 273 K for a System of 80 Molecules

Carbon Dioxide		Nitrogen		Water	
Percent (%)	D_s (cm^2/s)	Percent (%)	D_s (cm^2/s)	Percent (%)	D_s (cm^2/s)
5	0.00003974	95	0.0002653	0	N/A
10	0.0001619	85	0.0002862	5	0.0001172
10	0.00003816	90	0.0002704	0	N/A
15	0.00007887	85	0.0002494	0	N/A
50	0.00008877	50	0.0003038	0	N/A
100	0.0001018	0	N/A	0	N/A

The diffusion coefficients of carbon dioxide in flue gas mixture were also analyzed at 273 K, as shown in Table 11. At 273 K, the diffusion coefficient of carbon dioxide decreased. The composition of carbon dioxide and nitrogen in the flue gas mixture are varied, but the total volume remained constant. In addition, the temperature remained constant at 273K. The diffusion rates of carbon dioxide are slower when temperature is reduced from room temperature to 273K. For instance, at 298K, 15 mol% carbon dioxide in flue gas, which is 12 carbon dioxide molecules, diffuses at 0.00012 cm^2/s in IRMOF-1, and an equivalent mole percent composition of carbon dioxide in flue gas at 273 K diffuses at 0.00007887 cm^2/s in IRMOF-1. Similar behavior was observed for nitrogen. The results demonstrate that the diffusion coefficient is a function of temperature. In addition, the molecules travel slower as temperature is reduced since kinetic energy decreases as temperature decreases.

The diffusion coefficients of nitrogen, carbon dioxide, and water were determined at higher temperatures. Table 12 shows a diffusion coefficient of carbon dioxide of 0.000152 cm^2/s when the ternary mixture is at 353 K. If the temperature of ternary mixture is reduced to 313 K, a significant change will occur in diffusion coefficients. The diffusion coefficient of carbon dioxide at 353 K decreased when the temperature decreased to 313 K. The diffusion coefficient of nitrogen remained constant when the temperature decreased to 313 K. The illustrations of selectivity for CO_2 as a function of temperature shown previously agree with diffusion data because an increase in temperature resulted in high diffusion rates for carbon dioxide. The high diffusion rates can be attributed to weak adsorption of carbon dioxide in the metal sites.

Table 12: Diffusion Coefficient of Carbon Dioxide, Nitrogen, and Water in IRMOF-1 at 313 K and 353 K for a System of 80 Molecules

Temperature (313 K)	Carbon Dioxide		Nitrogen		Water	
	Percent (%)	D_s (cm^2/s)	Percent (%)	D_s (cm^2/s)	Percent (%)	D_s (cm^2/s)
	10	0.000134	85	0.000351	5	0.0000372
	15	0.000120	85	0.000343	0	N/A
Temperature (353 K)	Carbon Dioxide		Nitrogen		Water	
	Percent (%)	D_s (cm^2/s)	Percent (%)	D_s (cm^2/s)	Percent (%)	D_s (cm^2/s)
	10	0.000152	85	0.000349	5	0.000540

Table 13: Diffusion Coefficients of Carbon Dioxide, Nitrogen, and Water in Cu-BTC at 298K for a System of 80 Molecules

Carbon Dioxide		Nitrogen		Water	
Percent (%)	D_s (cm^2/s)	Percent (%)	D_s (cm^2/s)	Percent (%)	D_s (cm^2/s)
5	0.0000397	95	0.000192	0	N/A
10	0.00004867	85	0.00019511	5	0.00005090
10	0.00002542	90	0.0002133	0	N/A
15	0.00007800	85	0.0002020	0	N/A

The diffusion coefficient of carbon dioxide decreased when mole percent composition decreased as seen in Table 13. The diffusion coefficient of nitrogen increased when mole percent composition of nitrogen increased, as shown in Table 13. The diffusion rate decreased when temperature decreased for carbon dioxide and nitrogen. Carbon dioxide diffused slower in Cu-BTC at 273K and 298K, as shown in Table 14, but diffused faster in IRMOF-1 at 273K and 298K because Cu-BTC adsorption sites strongly adsorbed CO_2 for a longer time than IRMOF-1 adsorption sites. Similar behavior occurs for nitrogen in IRMOF-1 and Cu-BTC. Nitrogen diffused at a slower rate in Cu-BTC and diffused faster in IRMOF-1 at temperatures of 298K and 273K.

Table 14: Diffusion Coefficients of Carbon Dioxide, Nitrogen, and Water in Cu-BTC at 273K for a System of 80 Molecules

Carbon Dioxide		Nitrogen		Water	
Percent (%)	D_s (cm^2/s)	Percent (%)	D_s (cm^2/s)	Percent (%)	D_s (cm^2/s)
10	0.00001645	85	0.0001682	5	3.73×10^{-7}
10	0.00002567	90	0.0001370	0	N/A
15	0.00003688	85	0.0001840	0	N/A

The diffusion rate of carbon dioxide in Cu-BTC was slower than in IRMOF-1 at 298K for flue gas mixtures containing carbon dioxide and nitrogen. The diffusion rate of carbon dioxide in Cu-BTC was slower because the adsorption sites of Cu-BTC strongly adsorb carbon dioxide molecules. On the other hand, carbon dioxide molecules diffuse faster in IRMOF-1. The adsorption strength increased as the diffusion coefficient decreased. Moreover, the diffusion rates of nitrogen in IRMOF-1 are higher than the diffusion rates of nitrogen in Cu-BTC for flue gas mixtures where the total number of molecules is 80 molecules. The presence of water in flue gas mixtures resulted in a change in diffusion coefficients for carbon dioxide and nitrogen. When 5 mol% of water is present in flue gas, the diffusion rate of water in IRMOF-1 is 0.000197 cm^2/s. If more water was present in flue gas and less carbon dioxide was present, the diffusion rate of water decreased because IRMOF-1 adsorption sites were adsorbing more water molecules.

The diffusion coefficients of CO_2, N_2, and H_2O were determined at 313 K in ternary and binary mixtures that passed through Cu-BTC. From Table 15, we can observe that the diffusion coefficient of CO2 and water increased significantly from a temperature of 273 K to 313 K because the kinetic velocity of these molecules increased.

Table 15: Diffusion Coefficients of Carbon Dioxide, Nitrogen, and Water in Cu-BTC at 313 K for a System of 80 Molecules

Carbon Dioxide		Nitrogen		Water	
Percent (%)	D_s (cm^2/s)	Percent (%)	D_s (cm^2/s)	Percent (%)	D_s (cm^2/s)
10	0.0000457	85	0.000204	5	0.0000156
15	0.0000510	85	0.000217	0	N/A

The diffusion coefficients of CO_2, N_2, and water decrease as temperature decreases but increase as temperature increases, as shown in Tables 16-18 for flue gas at 273 K, 298 K, and 353 K in MIL-47. Furthermore, the diffusion of carbon dioxide, nitrogen, and water in flue gas flowing in MIL-47 are lower than Cu-BTC and IRMOF-1 at 298 K, 273 K, and 353 K compared at these temperatures and compositions with Cu-BTC and IRMOF-1. As a result, the diffusion of carbon dioxide, nitrogen, and water is slower in MIL-47 because the gas molecules are strongly adsorbing and interacting with the vanadium metal atoms in MIL-47.

Table 16: Diffusion Coefficients of Carbon Dioxide, Nitrogen, and Water in MIL-47 at 298K for a System of 80 Molecules

Carbon Dioxide		Nitrogen		Water	
Percent (%)	D_s (cm^2/s)	Percent (%)	D_s (cm^2/s)	Percent (%)	D_s (cm^2/s)
10	0.00000442	85	0.0000267	5	0.00000118
15	0.00000629	85	0.0000268	0	N/A

Table 17: Diffusion Coefficients of Carbon Dioxide, Nitrogen, and Water in MIL-47 at 273K for a System of 80 Molecules

Carbon Dioxide		Nitrogen		Water	
Percent (%)	D_s (cm^2/s)	Percent (%)	D_s (cm^2/s)	Percent (%)	D_s (cm^2/s)
10	0.000000670	85	0.0000185	5	0
15	0.00000157	85	0.0000163	0	N/A

Table 18: Diffusion Coefficients of Carbon Dioxide, Nitrogen, and Water in MIL-47 at 353 K for a System of 80 Molecules

Carbon Dioxide		Nitrogen		Water	
Percent (%)	D_s (cm^2/s)	Percent (%)	D_s (cm^2/s)	Percent (%)	D_s (cm^2/s)
10	7.21×10^{-6}	85	0.0000427	5	5.66×10^{-7}
15	0.0000120	85	0.0000488	0	N/A

Figure 30 shows diffusion coefficient of nitrogen decreasing at first for small number of molecules in the system, but as the number of molecules of nitrogen increased to larger values the diffusion coefficient increased and remained constant. The molecular weight of carbon dioxide is 44 g/mol, and the molecular weight of nitrogen is 28 g/mol.

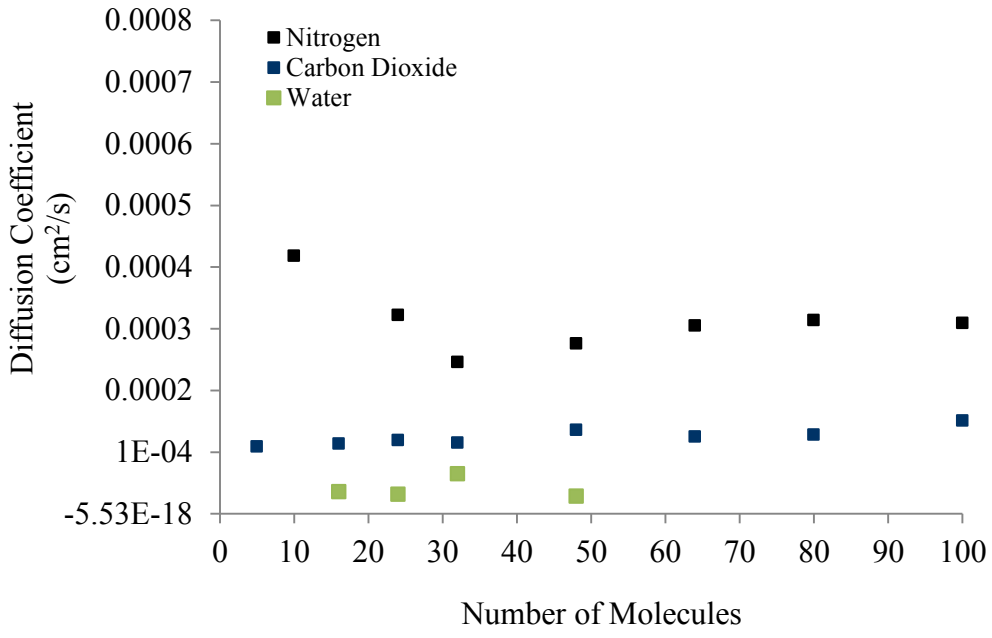

Figure 30. Diffusion coefficient as a function of number of molecules (CO_2, N_2, and H_2O) in IRMOF-1 at 298K.

Gas molecules with small mass have higher velocities. The molecular weight of nitrogen is lower in relation to the molecular weight of carbon dioxide. As a result, nitrogen has larger diffusion coefficients and diffuses faster in IRMOF-1. IRMOF-1 adsorbed more CO_2 than N_2 because carbon dioxide has a high quadrupole moment. Strong electrostatic interactions exist between CO_2 molecules and the metal sites of the metal-organic frameworks, which results in large pore size differences.[30]

The self-diffusivities of gas molecules were also investigated for carbon dioxide, nitrogen, and water in Cu-BTC. The self-diffusion coefficient of a component *i* was analyzed as the number of molecules of component *i* increased as well. Figure 31 shows the self-diffusion coefficient of carbon dioxide and nitrogen increasing initially as the number of molecules in a 2 × 2 × 2 Cu-BTC cubic unit cell increases.

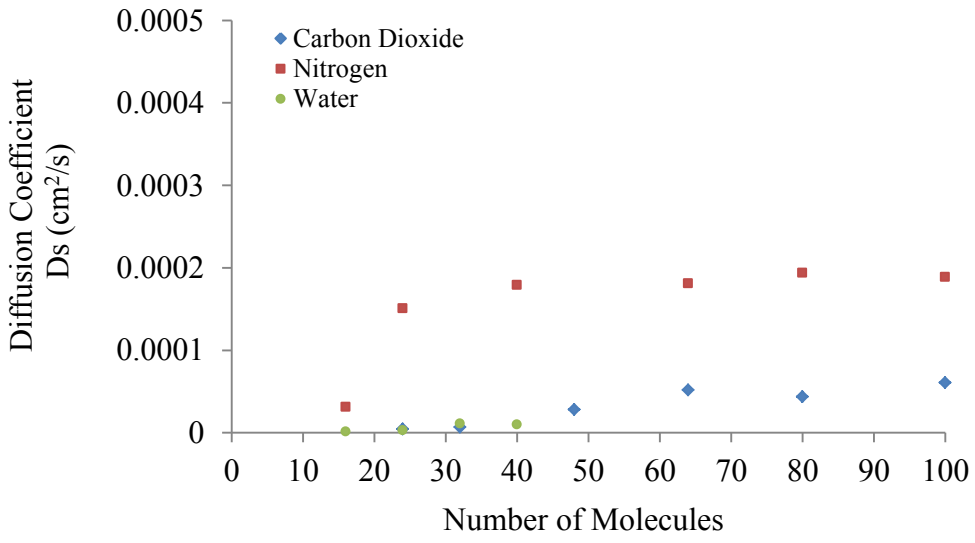

Figure 31. Diffusion coefficient as a function of the number of molecules (CO_2, N_2, and H_2O) in Cu-BTC at 298K.

The diffusion coefficient remains constant at higher number of molecules. The diffusion coefficient of carbon dioxide is lower when carbon dioxide adsorbs in Cu-BTC at 298K than IRMOF-1 because metal sites of Cu-BTC adsorb carbon dioxide for a longer time. Carbon dioxide diffuses faster in IRMOF-1 at 298K. The diffusion coefficient of carbon dioxide in Cu-BTC at 298K increases as the number of molecules increases. In Figure 31, the self-diffusion coefficient of carbon dioxide is lower than the self-diffusion coefficient of nitrogen. The nitrogen diffused faster than carbon dioxide because nitrogen was weakly adsorbed in Cu-BTC, whereas carbon dioxide was strongly adsorbing in the metal sites of Cu-BTC as a result of the quadrupole moment of CO_2. A more thorough analysis was performed for a specific number of molecules in MOFs. Table 19-21 show the diffusion coefficients of 100 mol% of CO_2, N_2, and H_2O in Cu-BTC, IRMOF-1, and MIL-47. The self-diffusion coefficient of each component was obtained after a period of 10 ns at 273 K, 298K, and 313 K.

Table 19: Diffusion Coefficients of 100 mol% (24 molecules) of CO_2, N_2, and H_2O in IRMOF-1

Component	T=273K D_s (cm^2/s)	T=298K D_s (cm^2/s)	T=313K D_s (cm^2/s)
Nitrogen	0.000248	0.000322	0.000309
Carbon Dioxide	0.0000856	0.000119	0.000120
Water	0.0000175	0.0000329	0.0000346

Table 20: Diffusion Coefficients of 100 mol% (24 molecules) of CO_2, N_2, and H_2O in Cu-BTC

Component	T=273K D_s (cm^2/s)	T=298K D_s (cm^2/s)	T=313K D_s (cm^2/s)
Nitrogen	0.000148	0.000151	0.000151
Carbon Dioxide	0.000000810	0.00000159	0.00000164
Water	0.00000138	0.000003113	0.00000231

Table 21: Diffusion Coefficients of 100 mol% (24 molecules) of CO_2, N_2, and H_2O in MIL-47

Component	T=273K D_s (cm^2/s)	T=298K D_s (cm^2/s)	T=313K D_s (cm^2/s)
Nitrogen	0.0000176	0.00002849	0.0000676
Carbon Dioxide	0.000000437	0.000000522	0.00000180
Water	0.000000132	0.000000613	2.11×10^{-7}

Based on the MD simulations and the mean-square displacement method, carbon dioxide is strongly adsorbed in MIL-47 at room temperatures and low and high temperatures. In addition, the adsorption of carbon dioxide is stronger in Cu-BTC than IRMOF-1 because the diffusion coefficient of CO_2 is smaller when strong adsorption occurs. Lastly, the diffusion coefficient of CO_2, N_2, and H_2O increased slightly as temperature increased.

Radial distribution functions

The radial distribution functions of carbon dioxide, nitrogen, water, and metal atoms in MOFs were obtained using MD simulations and DL_Poly after a simulation period of 50 ns. The radial distribution function provides information about the density of a particular particle with respect to another particle. In a crystal, the radial distribution function g(r) has sharp spikes. The sharp pikes indicate the certainty that molecules lie at definite locations. In a liquid state, g(r) loses the periodic array of sharp peaks.[20] The pair radial distribution function for a flue gas mixture with composition 15 mol% CO_2 and 85 mol% N_2 in IRMOF-1 at 298K is shown in Figure 32.

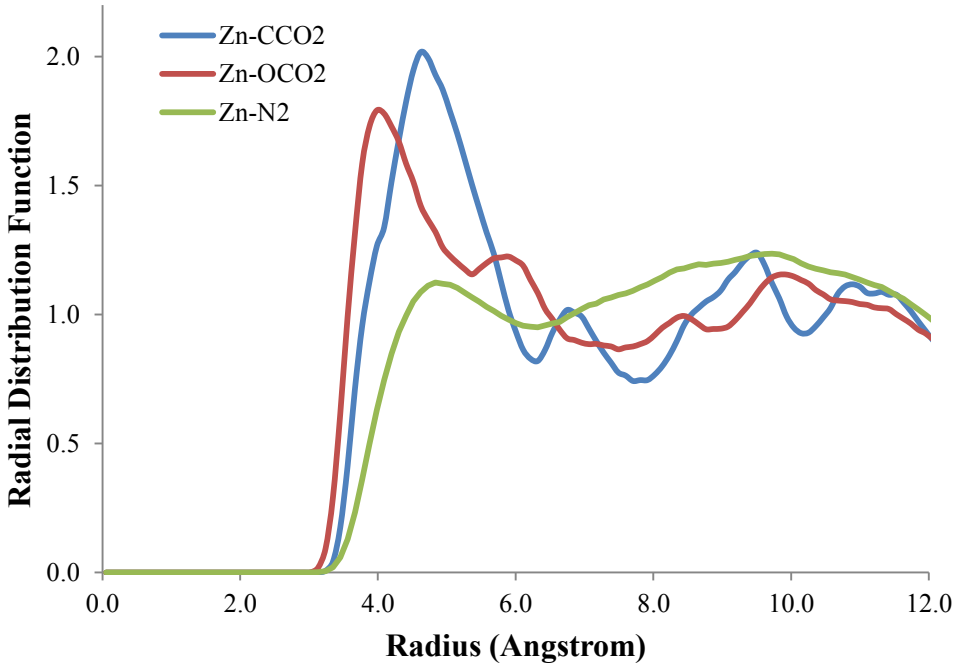

Figure 32. The radial distribution function of Zn-CCO_2, Zn-OCO_2, and Zn-N_2 for an 85 mol% N_2 and 15 mol% CO_2 mixture at 298 K in IRMOF-1.

Figure 32 shows differences in the density of carbon dioxide atoms and nitrogen atoms as a function of the radial distance from zinc atom. The peaks indicate the location of an atom from the reference atom. Figure 4 shows fluctuations but the peaks are not sharp. The reason is that nitrogen and carbon dioxide are not in the solid state. For the Zn-OCO_2 species, the peak is located at 3.98 Å. The next peak is located at 4.6 Å, which corresponds to the Zn-CCO2 species. The Zn-N2 is also located at 4.6 Å. The radial distribution function of Zn-N2 has fewer sharp peaks. Furthermore, from Figure 32, we can see that zinc strongly interacts with the oxygen atom in CO_2 because the peak is located a smaller radial distance. The radial distribution function was obtained for a flue gas with composition of 90 mol% N_2 and 10 mol% CO_2 in IRMOF-1 at 298 K, which is shown in Figure 33.

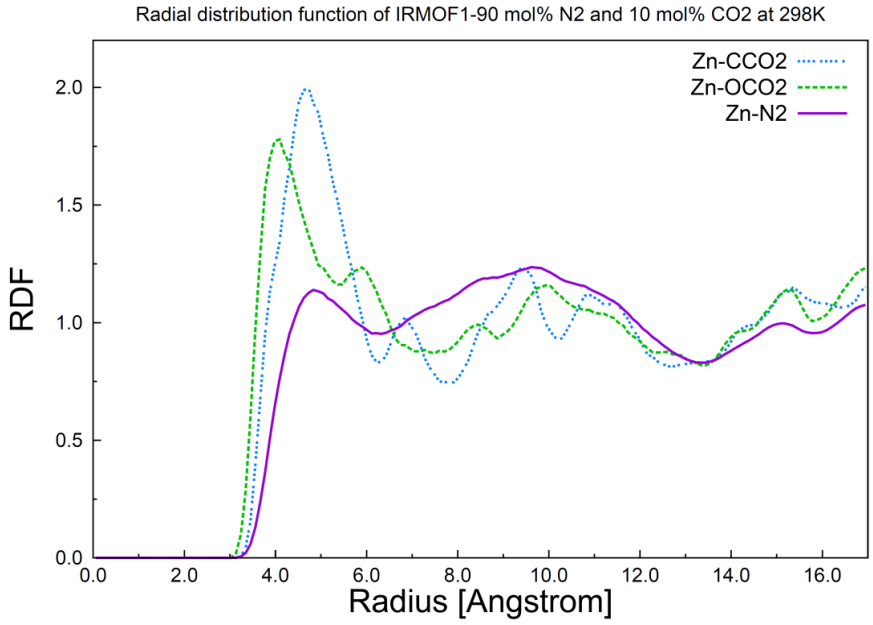

Figure 33. The radial distribution function of Zn-CCO_2, Zn-OCO_2, and Zn-N_2 for a 90 mol% N_2 and 10 mol% CO_2 mixture at 298 K in IRMOF-1.

Figure 32 and Figure 33 look relatively the same. Similar behavior is observed when the flue gas composition is changed by a small percentage. The presence of 5 mol% of water in the flue gas and the reduction of composition of CO_2 in flue gas did not cause a change in the RDF of the atomic pairs: Zn-CCO2, Zn-OCO2, and Zn-N2, as shown in Figure 34.

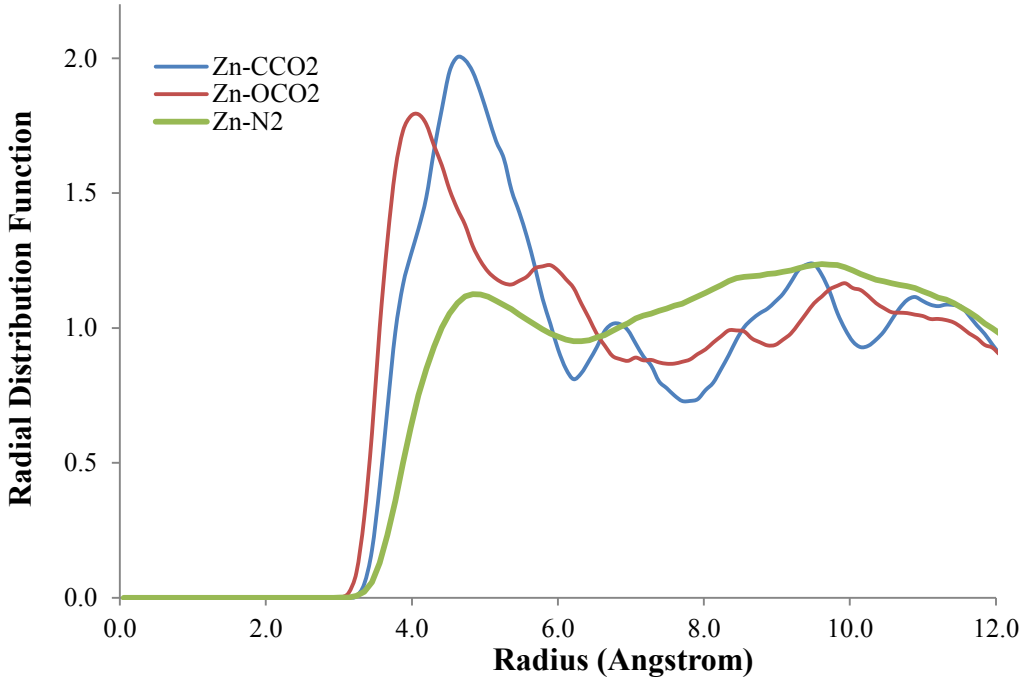

Figure 34. The radial distribution function of Zn-CCO_2, Zn-OCO_2, and Zn-N_2 for an 85 mol% N_2, 10 mol% CO_2, and 5 mol% H_2O mixture at 298K in IRMOF-1.

To determine if strong adsorption of water occurs in IRMOF-1, the RDF for the atomic pairs: Zn-H of H_2O and Zn-O of H_2O were obtained.

Figure 35 shows distinctive peaks for both atomic pairs. The nearest hydrogen atom in a water molecule is 3.1 Å from a zinc metal site, whereas the oxygen atom in a water molecule is found 4.0 Å away from the zinc metal site. Based on the figures shown, carbon dioxide and water compete for adsorption in zinc metal sites.

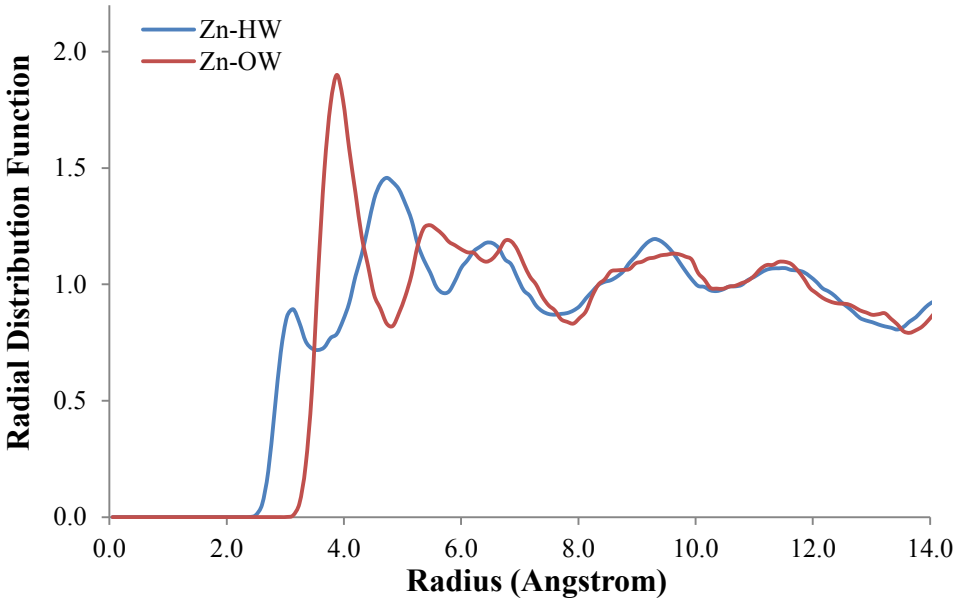

Figure 35. The radial distribution function of Zn-H (H_2O) and Zn-O (H_2O) for an 85 mol% N_2, 10 mol% CO_2, and 5 mol% H_2O mixture at 298K in IRMOF-1.

From Figure 35, we can conclude that the zinc atom is strongly interacting with the oxygen atom in the water molecule because the distance between the zinc and the nearest oxygen atom of a water molecule is smaller than the distance between the zinc and the atoms in N_2 and CO_2, which are shown in Figure 34. The arrangement of water molecules with respect to one another is verified in Figure 36. The oxygen atom is

located farther away to another oxygen atom in a water molecule. The hydrogen atoms in a water molecule are located closer to each compared to the distance between oxygen atoms. The red peak for the atomic pair HW-OW shows that the distance between hydrogen atoms and oxygen atoms is 1.75 Å, which is small when compared to the other atomic pairs.

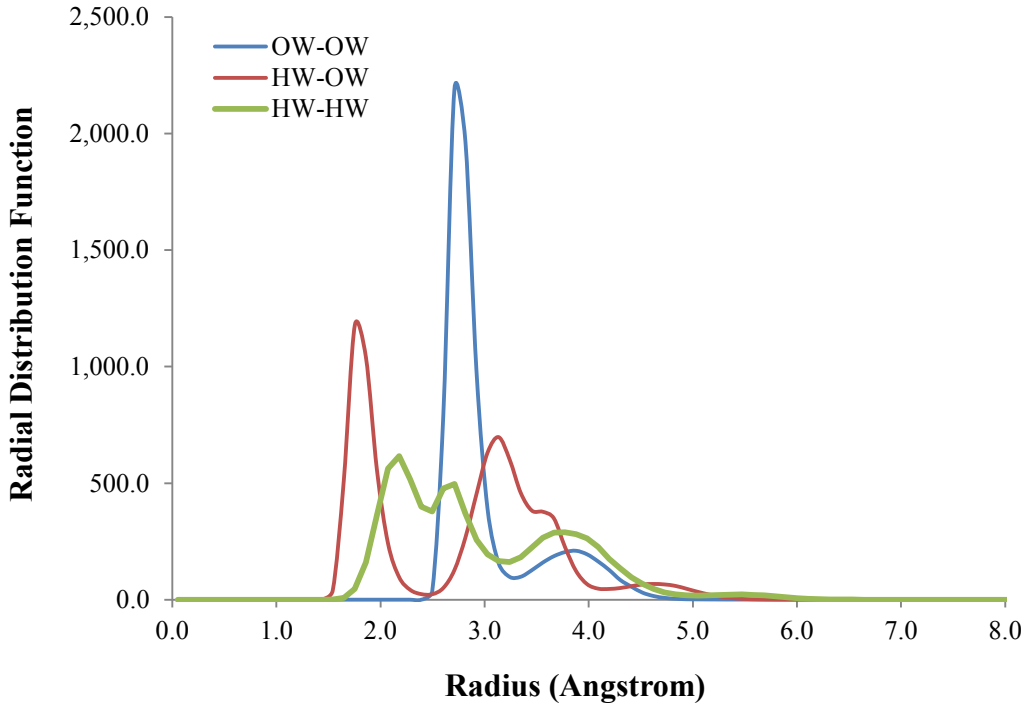

Figure 36. The radial distribution function of OW-OW, HW-OW, and HW-HW for an 85 mol% N_2, 10 mol% CO_2, and 5 mol% H_2O mixture at 298K in IRMOF-1.

Radial distribution functions were obtained for flue gas in Cu-BTC at 298 K. The first case analyzed in MD consisted of flue gas with a composition of 85 mol% N_2 and 15

mol% CO_2 flowing at 298 K in Cu-BTC. After the gas molecules interacted in Cu-BTC for a period of 50 ns, Figure 37 was obtained.

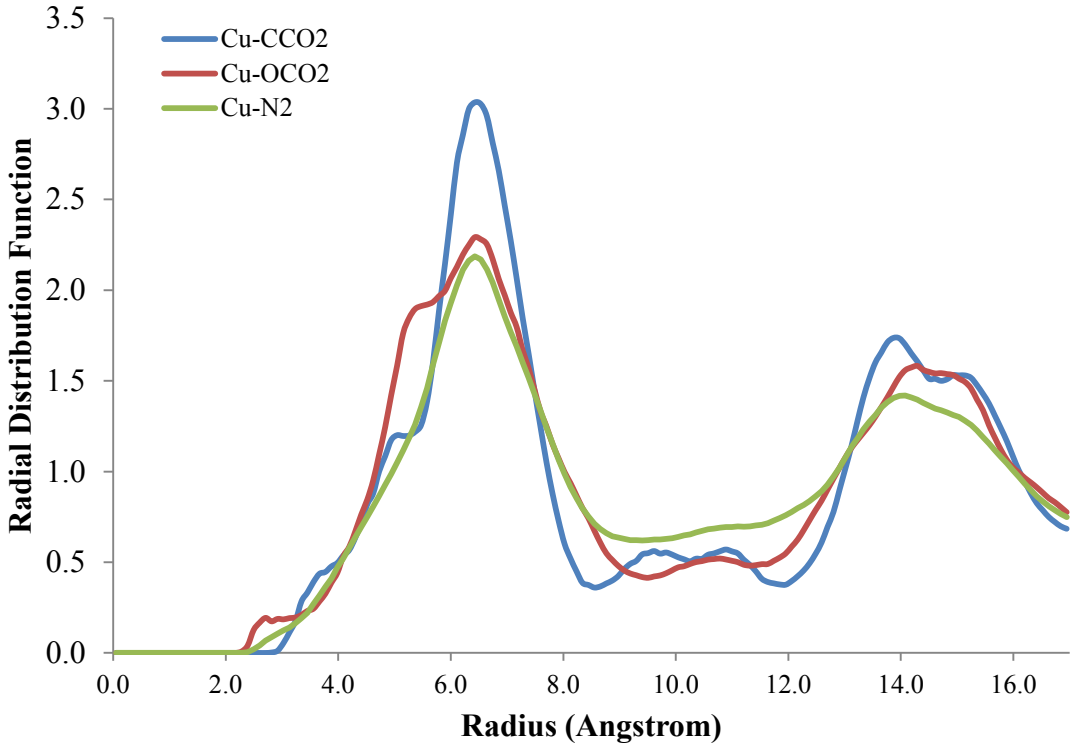

Figure 37. The radial distribution function of Cu-CCO_2, Cu-OCO_2, and Cu-N_2 for an 85 mol% N_2 and 15 mol% CO_2 mixture at 298K in Cu-BTC.

Figure 37 shows the location of oxygen atoms in CO_2 relative to the copper metal in Cu-BTC. The nearest carbon to a copper metal was located at 4.8 Å. The oxygen atom in carbon dioxide was closer to the copper metal because a small peak can be seen in Figure 37 at 2.62 Å. On the other hand, nitrogen atom in N_2 was located 6.2 Å from the copper metal in Cu-BTC. Based on Figure 37, copper metal was strongly adsorbing

carbon dioxide at 298 K for a period of 50 ns. Furthermore, the adsorption of carbon dioxide in Cu-BTC was stronger than the adsorption of carbon dioxide in IRMOF-1 for the same flue gas composition because an oxygen atom in CO_2 was found at 2.62 Å away from a copper atom whereas an oxygen atom in CO_2 was located at 4.62 Å from a zinc atom.

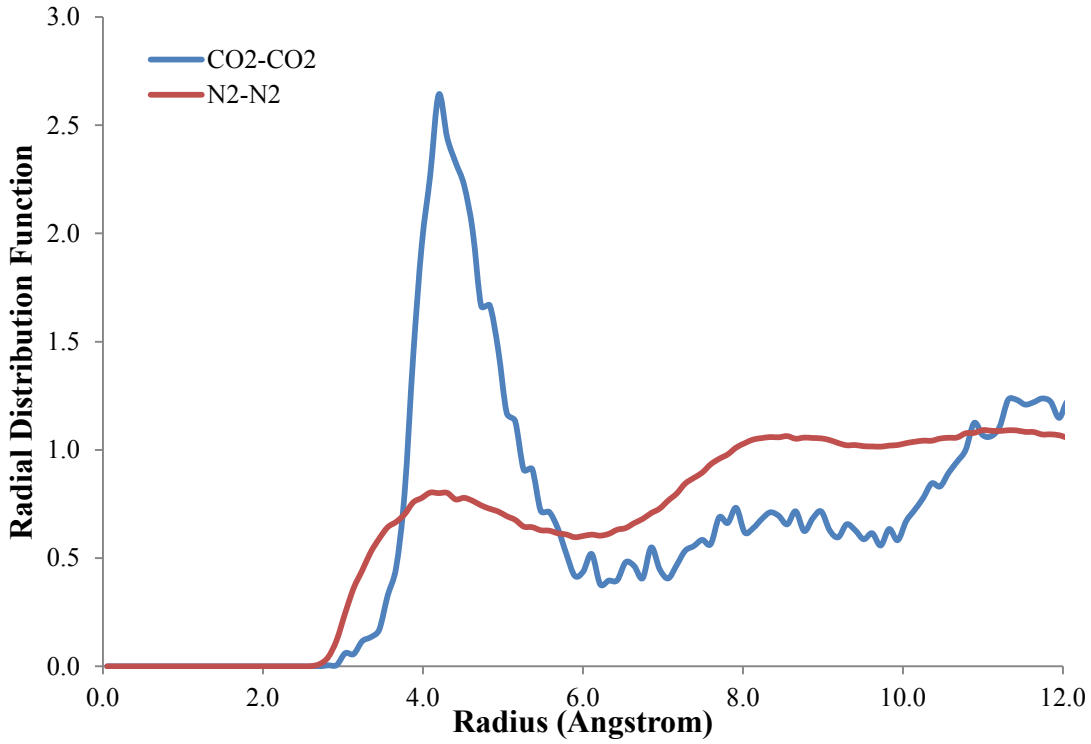

Figure 38. The radial distribution function of CCO_2-CCO_2 and N_2-N_2 for an 85 mol% N_2 and 15 mol% CO_2 mixture at 298K in Cu-BTC.

Figure 38 shows the location of carbon atoms in CO_2 relative to each other. The nearest carbon atom from another carbon atom in carbon dioxide was found at 4.2 Å. The

nearest nitrogen atom from another nitrogen was found at 3.98 Å. The behavior of the radial distribution function shows a non-solid state since the peaks are not sharp because the carbon dioxide and nitrogen molecules are in the gas phase. The radial distribution function was obtained for a flue gas with a higher composition in nitrogen (90 mol% N_2) to observe if any changes would occur in the RDF of each atomic pair. Figure 39 shows the RDF of the atomic pairs: Zn-CCO2, Zn-OCO2, Zn-N2. Based on Figure 39, the peaks are located at about the same radius when compared to Figure 37.

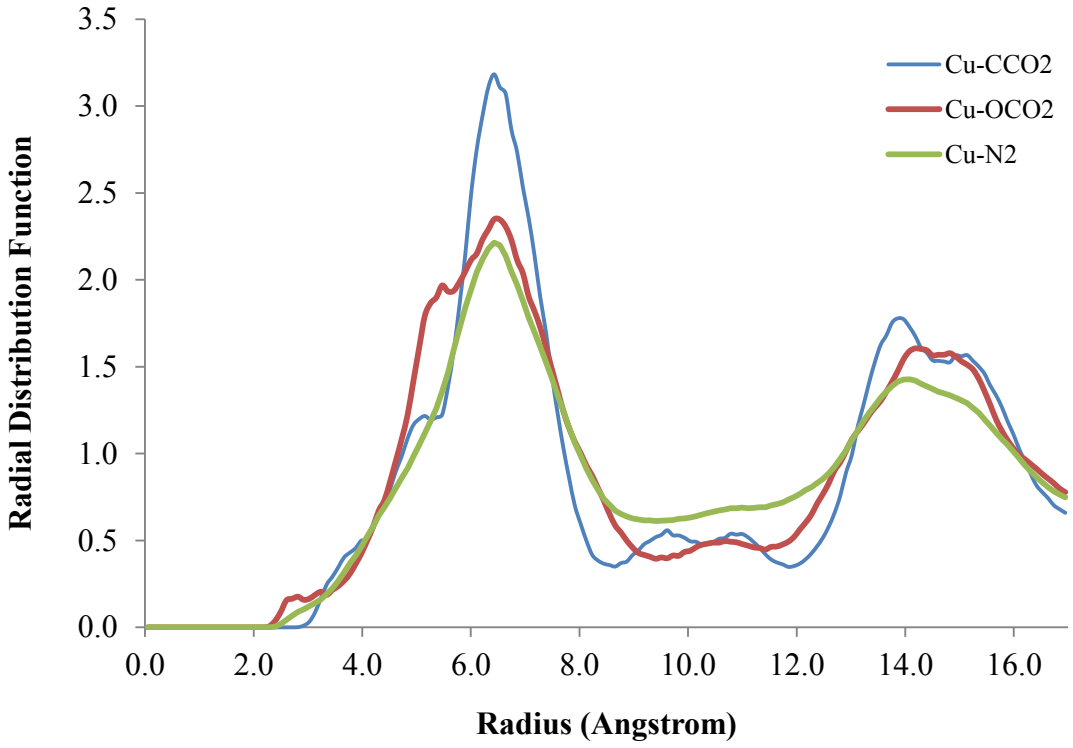

Figure 39. The radial distribution function of Cu-CCO_2, Cu-OCO_2, and Cu-N_2 for a 90 mol% N_2 and 10 mol% CO_2 mixture at 298K in Cu-BTC.

The RDF was determined for a flue gas with a composition of 5 mol% H_2O, 85 mol% N_2, and 10 mol% CO_2 flowing in Cu-BTC. Figure 40 shows the location of oxygen atoms in CO_2 relative to the copper metal in Cu-BTC. The nearest carbon to copper metal is located at 4.0 Å, whereas the nearest oxygen atom in carbon dioxide is 3.5 Å away from the copper metal. Based on Figure 40, the nitrogen atom is farther to the copper metal site.

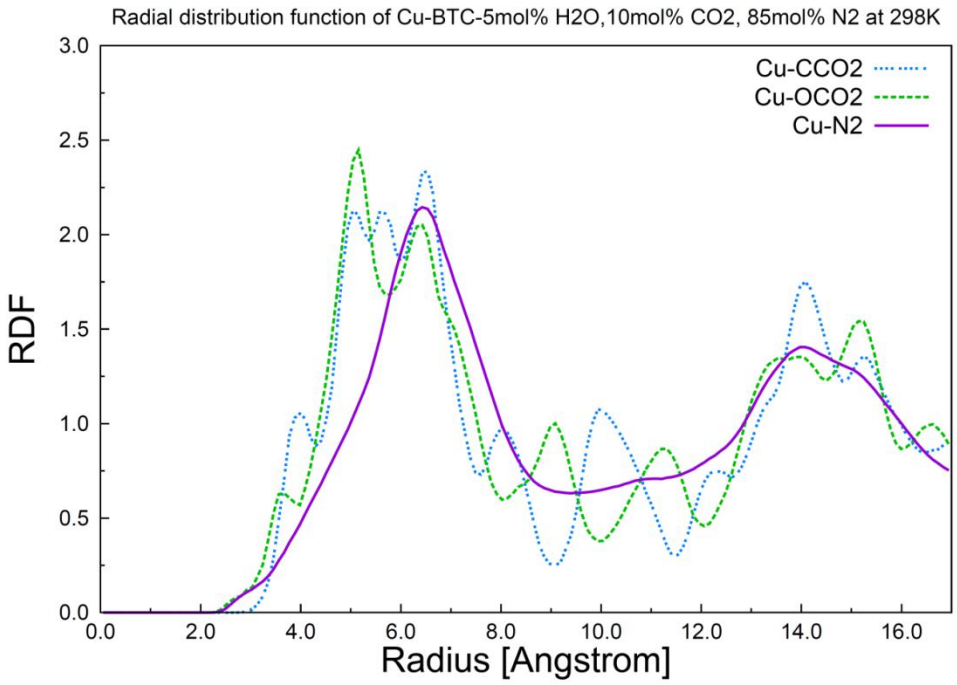

Figure 40. The radial distribution function of Cu-CCO_2, Cu-OCO_2, and Cu-N_2 for an 85 mol% N_2, 10 mol% CO_2, and 5 mol% H_2O mixture at 298K in Cu-BTC.

Figure 41 shows the location of oxygen atoms in H_2O relative to the copper metal in Cu-BTC and the location of hydrogen atoms in H_2O relative to the copper metal. The closest oxygen atom in water found radially away from copper is located 2.2 Å, and the hydrogen atom in water is found 3.0 Å from the copper metal. According to Figure 41, Cu-BTC strongly adsorbs water molecules than IRMOF-1 because the oxygen in a water molecule is closest to copper than zinc.

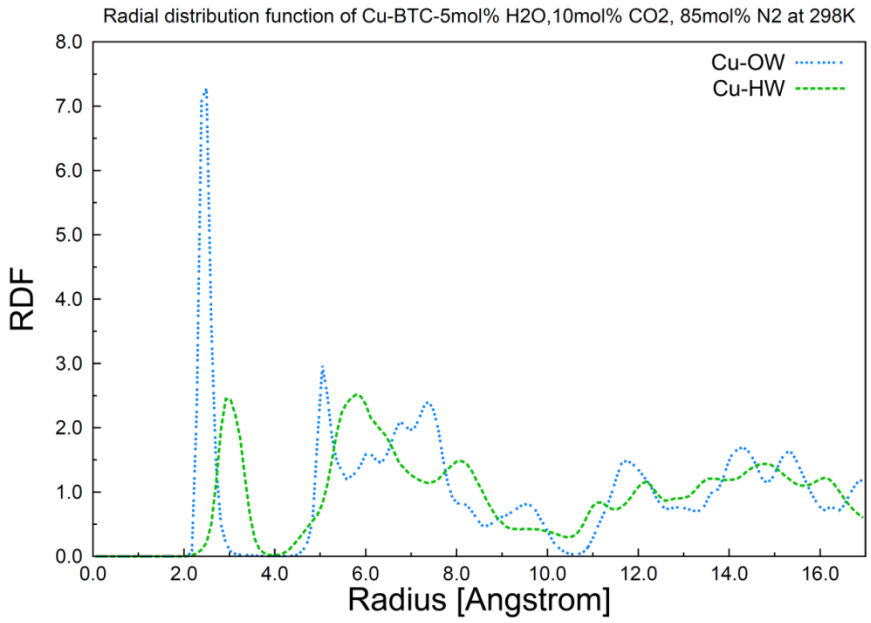

Figure 41. The radial distribution function of Cu-O (H_2O) and Cu-H (H_2O) for an 85 mol% N_2, 10 mol% CO_2, and 5 mol% H_2O mixture at 298K in Cu-BTC.

The pair radial distribution of V-CCO2, V-OCO2, and V-N2 were obtained for flue gas with composition of 85 mol% N_2 and 15 mol% CO_2 and another gas mixture with composition of 85 mol% N_2, 10 mol% CO_2, and 5 mol% H_2O. The flue gas was adsorbed in MIL-47 at 298 K at constant volume and constant number of molecules. The flue gas was simulated in MIL-47 at 298 K for a period of 15 ns in DL_POLY. Figure 42 shows peaks between 4.0 Å and 5.0 Å. Figure 42 shows the nearest carbon atom in CO_2 from vanadium atom at 4.4 Å. The Figure 42 shows the nearest oxygen atom in CO_2 from vanadium at 4.7 Å, and the nearest nitrogen atom in N_2 from vanadium at 4.8 Å. Figure 42 confirmed more adsorption of carbon dioxide in MIL-47 than nitrogen based on the radial distance of atomic pairs.

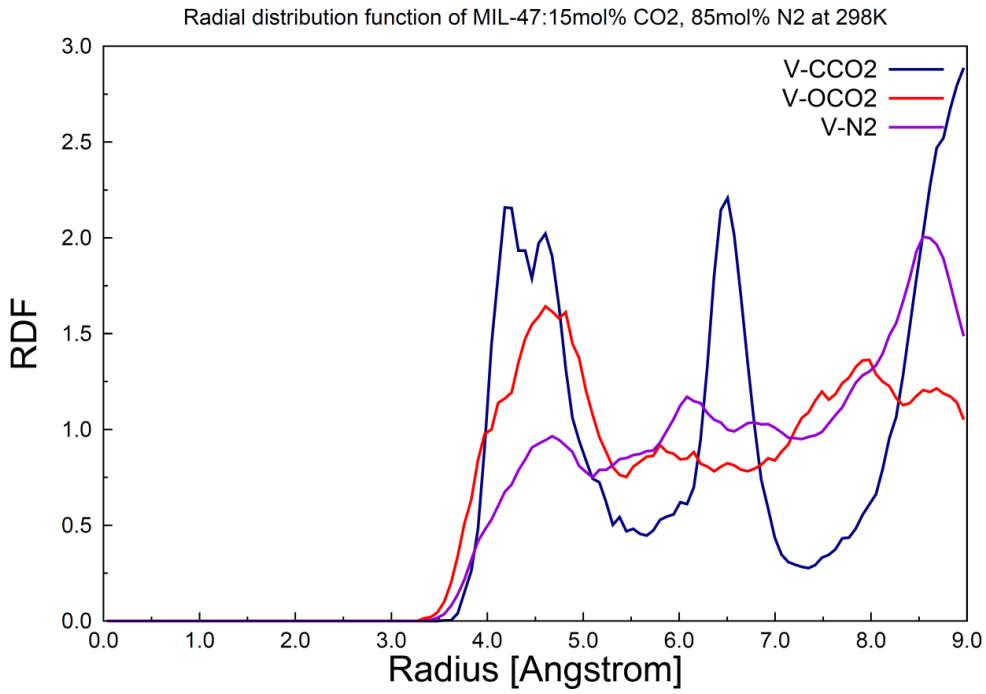

Figure 42. The radial distribution function of V-CCO2, V-OCO2, and V-N_2 for an 85 mol% N_2 and 15 mol% CO_2 mixture at 298K in MIL-47.

The atomic pair radial distribution functions for hydrogen atom in water and vanadium, as well as the oxygen in water and vanadium for a flue gas with a composition of 85 mol% N_2, 10 mol% CO_2, and 5 mol% H_2O are shown in Figure 43. Based on Figure 43, we can conclude that the hydrogen in the water molecule is closer to the vanadium atom in MIL-47 than the oxygen in the water molecule. However, the hydrogen atom in the water molecule and the oxygen atom in the water molecule were located closer to the vanadium metal when compared to the atoms in CO_2 and N_2; as a result, adsorption of water is stronger than carbon dioxide and nitrogen adsorption in MIL-47 at 298 K for flue gases with high compositions of N_2 and low compositions of H_2O and CO_2.

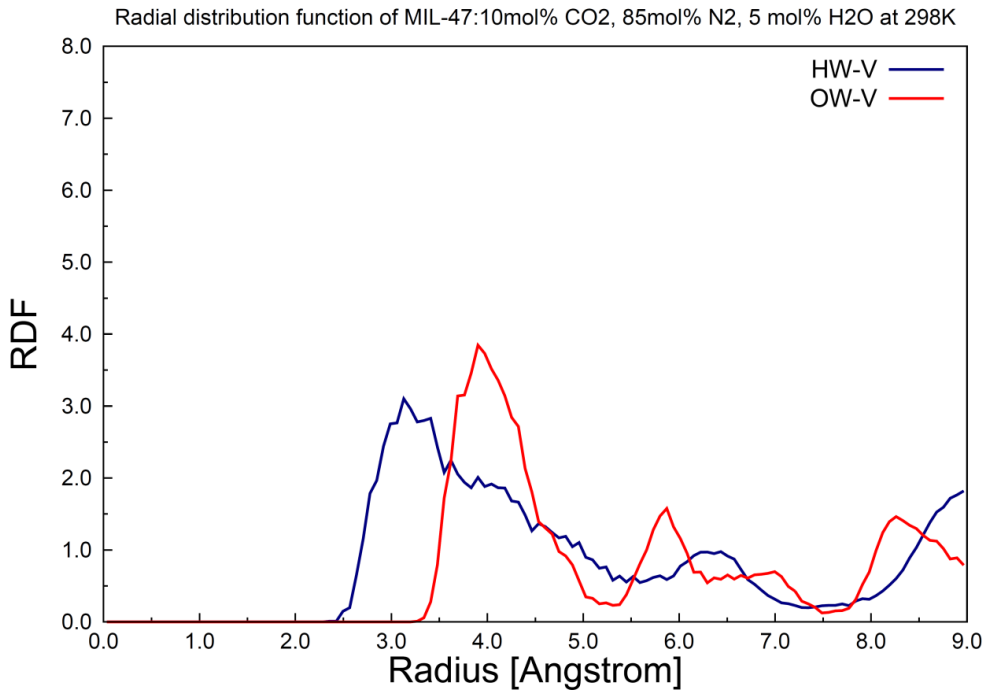

Figure 43. The radial distribution function of V-H (H_2O) and V-O (H_2O) for an 85 mol% N_2, 10 mol% CO_2, and 5 mol% H_2O mixture at 298K in MIL-47.

Figure 44 shows the pair RDFs of V-CCO2, V-OCO2, and V-N2 in ternary mixture at 298 K in MIL-47. From Figure 44, we can conclude that the position of carbon atom in carbon dioxide is 4.4 Å away from the vanadium metal in MIL-47, and the nitrogen atom in N_2 is farther from the vanadium metal in MIL-47 at 4.8 Å. Lastly, from Figure 44, we can see that carbon dioxide and nitrogen were equally adsorbed in MIL-47 at 298 K at the specified flue gas composition.

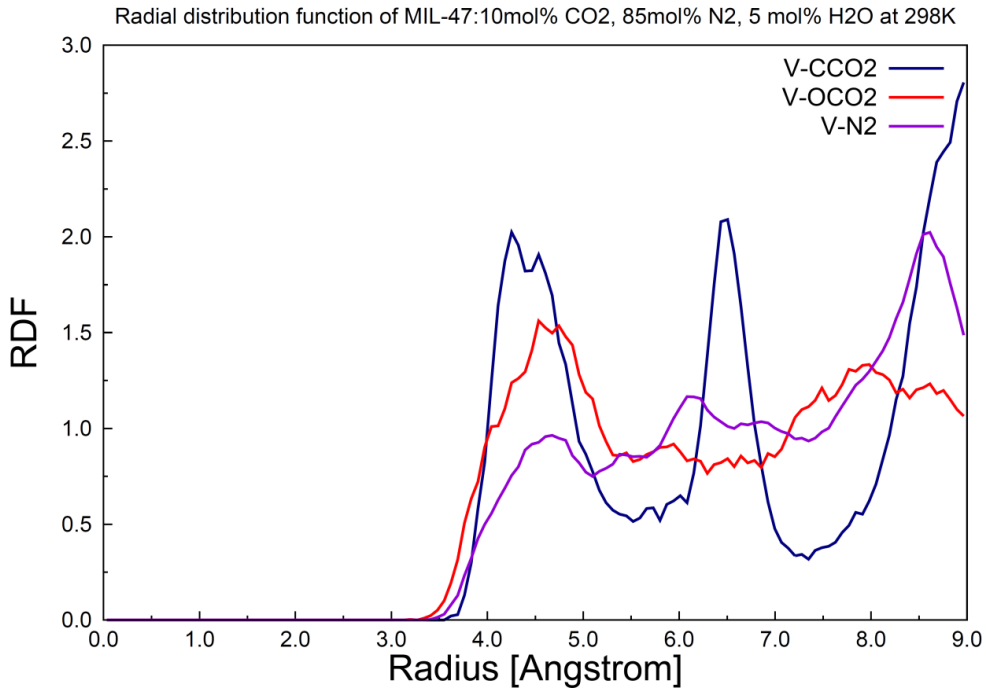

Figure 44. The radial distribution function of V-CCO2, V-OCO2, and V-N_2 for an 85 mol% N_2, 10 mol% CO_2, and 5 mol% H_2O mixture at 298K in MIL-47.

CHAPTER IV

SUMMARY AND CONCLUSIONS

The purpose of this study was to analyze gas adsorption in three MOFs: Cu-BTC, IRMOF-1, and MIL-47. The gas adsorption in MOFs was analyzed using Material Studio 5.5, DL_POLY, GCMC simulations, and Molecular Dynamics. The guest molecules in flue gas were CO_2, N_2, and H_2O. Ternary and binary mixtures were separately investigated at various temperatures. The goal of the project was to analyze the selectivity for CO_2 in MOFs. The selectivity for CO_2 was obtained from the amount of CO_2 and N_2 adsorbed at specific temperatures.

Selectivity for carbon dioxide

Overall, MIL-47 had the highest selectivity for CO_2 at room temperature (298 K), whereas Cu-BTC had a higher selectivity for CO_2 than IRMOF-1. The selectivity for CO_2 in MIL-47 at 4000 kPa and 298 K was 26.5, and the selectivity in Cu-BTC at the same temperature and pressure conditions was 18. The least selective MOF was IRMOF-1 because the selectivity for CO_2 at 4000 kPa and 298 K was 12. In the presence of water, the selectivity for CO_2 for all MOFs increased; however, for MIL47, the selectivity for CO_2 could not be determined for statistical reasons.

Diffusion coefficients

The diffusion of CO_2, N_2, and H_2O were analyzed using the mean-square displacement method, which provided information about the movement of guest molecules in MOFs. Based on the diffusion coefficients gathered for each MOF at various temperatures, the diffusion of carbon dioxide was slower than the diffusion of nitrogen in IRMOF-1, MIL-47, and Cu-BTC because carbon dioxide has a quadrupole moment that causes the CO_2 molecule to strongly interact with the metal sites in MOFs. When water was present in flue gas, the diffusion coefficient of water was smaller than CO_2 and N_2, which signified that water was strongly interacting with the metal sites in the MOFs. The diffusion coefficient of CO_2, N_2, and H_2O increased as temperature was increased from 273 K to 313 K because the kinetic velocity of the guest molecule increased with temperature.

Radial distribution functions

The RDFs studied in this project indicated the location of CO_2, H_2O, and N_2 with respect to the metal sites in MOFs. Based on the RDFs obtained from MD simulations, we can conclude that the atoms in H_2O were closer to the metal sites in MIL-47, Cu-BTC, and IRMOF-1 at room temperature than the atoms in CO_2 and N_2 because water was strongly interacting with vanadium, copper, and zinc in the MOFs. As a result, the adsorption of CO_2 in flue gases that contain water is low in MOFs. To have a higher adsorption of CO_2 in flue gases, the water should be removed prior to sending the flue gas to a MOF adsorption system. Overall, MOF systems can be integrated in coal-fired plants to remove CO_2 gases; however, the physical properties of MOFs can be tuned to increase the selectivity for CO_2 and efficiently remove CO_2 in flue gases.

REFERENCES

(1) Lackner, K. S. *Issues in Environmental Science and Technology* **2010**, *29*.

(2) Figueroa, J. D.; Fouth, T.; Plasynski, S.; McIlvried, H.; Srivastava, R. D. *International Journal of Greenhouse Gas Control* **2007**, *2*, 9-20.

(3) Xie, X.; Economides, M. J. *Journal of Natural Gas Science and Engineering* **2009**, *1*, 103.

(4) Robertson, E. P. *International Journal of Coal Geology* **2009**, *77*, 234-241.

(5) Sioshanshi, F., Generating Electricity in a Carbon-Constrained World, Elsevier: San Diego, 2010; pp 127-174.

(6) Li, J.-R.; Ma, Y.; McCarthy, M. C.; Sculley, J.; Yu, J.; Jeong, H.-K.; Balbuena, P. B.; Zhou, H.-C. *Coordination Chemical Reviews* **2011**, *255*, 1791.

(7) Termuehlen, H.; Empsperger, W. *Clean and Efficient Coal Fired Power Plants*; ASME Press: New York, 2003.

(8) Cutlip, L.; Fath, B. D. *Environment, Development and Sustainability* **2011**, 1.

(9) Giavarini, C.; Maccioni, F.; Santarelli, M. L. *Fuel* **2010**, *89*, 623.

(10) Li, J.-R.; Kuppler, R. J.; Zhou, H.-C. *The Royal Society of Chemistry* **2008**, *38*, 1477.

(11) Getman, R. B.; Miller, J. H.; Wang, K.; Snurr, R. Q. *Journal of Physical Chemistry C* **2011**, *115*, 2066.

(12) Geankoplis, C. J. *Transport Processes and Separation Process Principles*, 4th ed.; Prentice Hall: Upper Saddle River, New Jersey, 2003.

(13) Environmental Protection Agency. Adsorption. http://www.epa.gov/apti/Materials/APTI%20415%20student/415%20Student%20Manual/415_Chapter_4_12-15-2008.pdf . 2008. (accessed 20 November 2011).

(14) Liu, B.; Smit, B. *Langmuir* **2009**, *25*, 5918.

(15) Dubbeldam, D.; Frost, H.; Walton, K. S.; Snurr, R. Q. *Fluid Phase Equilibria* **2007**, *261*, 152.

(16) Chmelik, C.; Karger, J.; Wiebcke, M.; Caro, J.; Baten, J. M. v. *Microporous and Mesoporous Materials* **2009**, 22-32.

(17) Gupta, A.; Chempath, S.; Sanborn, M. J.; Clark, L. A.; Snurr, R. Q. *Molecular Simulation* **2003**, *29*, 29.

(18) Chempath, S.; Clark, L. A.; Duren, T.; Gupta, A.; Sanborn, M. J.; Sarkisov, L. Music Documentation. http://zeolites.cqe.northwestern.edu/Music/Documentation index.html. 2003. (accessed 24 May 2011).

(19) Quantumwise. Geometry of a Water Molecule. http://www.quantumwise.com/ /documents/manuals/ATK-2008.10/chap.simplemol.html. (accessed 29 June 2011).

(20) Atkins, P.; Paula, J. d. *Atkins' Physical Chemistry*, 8th ed.; W.H. Freeman and Company: New York, New York, 2006.

(21) Mayo, S. L.; Olafson, B. D.; Goddard, W. A. *Journal of Physical Chemistry* **1990**, *94*, 8897.

(22) Potoff, J. J.; Siepmann, J. I. *AIChE* **2011**, *47*, 1676.

(23) Berendsen, H. J. C.; Grigera, J. R.; Straatsma, T. P. *Journal of Physical Chemistry* **1987**, *91*, 6269.

(24) Al-Matar, A. K.; Rockstraw, D. A. *Journal of Computational Chemistry* **2004**, *25*, 660.

(25) Farrusseng, D.; Daniel, C.; Gaudillere, C.; Ravon, U.; Schuurman, Y.; Mirodatos, C.; Dubbeldam, D.; Frost, H.; Snurr, R. Q. *Langmuir* **2009**, *25*, 7383.

(26) Salles, F.; Jobic, H.; Devic, T.; Llewellyn, P. L.; Serre, C.; Ferey, G.; Maurin, G. *ACS Nano* **2009**, *4*, 143.

(27) Smith, W.; Todorov, I. T. *Molecular Simulation* **2006**, *32*, 935.

(28) Smith, W.; Forester, T. R. *Journal of Molecular Graphics* **1996**, *14*, 136.

(29) Smith, W.; Yong, C. W.; Rodger, P. M. *Molecular Simulation* **2002**, *28*, 385.

(30) Karra, J. R.; Krista, W. S. *Journal of Physical Chemistry C* **2010**, *114*, 15735.

CONTACT INFORMATION

Name:	Hilda A. Mera Student
Professional Address:	c/o Dr. Perla Balbuena Department of Chemical Engineering MS 4227 Texas A&M University College Station, TX 77843
Email Address:	hmera511@tamu.edu
Education:	B.S., Chemical Engineering, Texas A&M University, May 2012 Undergraduate Research Scholar Phi Kappa Phi